Rate-Energy Region of SWIPT for MIMO Broadcasting Under Nonlinear Energy Harvesting Model

Ke Xiong, *Member, IEEE*, Beibei Wang, *Senior Member, IEEE*, and K. J. Ray Liu, *Fellow, IEEE*

***Abstract*— This paper explores the rate-energy (R-E) region of simultaneous wireless information and power transfer for MIMO broadcasting channel under the nonlinear radio frequency energy harvesting (EH) model. The goal is to characterize the tradeoff between the maximal energy transfer versus information rate. The separated EH and information decoding (ID) receivers and the co-located EH and ID receivers scenarios are considered. For the co-located receivers scenario, both time switching (TS) and power splitting (PS) receiver architectures are investigated. Optimization problems are formulated to derive the boundaries of the R-E regions for the considered systems. As the problems are nonconvex, we first transform them into equivalent ones and derive some semi-closed-form solutions, and then design efficient algorithms to solve them. Numerical results are provided to show the R-E regions of the systems, which provide some interesting insights. It is shown that all practical circuit specifications greatly affect the system R-E region. Compared with the systems under traditional linear EH model, the ones under the nonlinear EH model achieve smaller R-E regions due to the limitations of practical circuit features and also show very different R-E tradeoff behaviors.**

***Index Terms*— Simultaneous wireless information and power transfer, MIMO, rate-energy region, rate-energy tradeoff, nonlinear energy harvesting model.**

I. Introduction

RECENTLY, radio frequency (RF) energy harvesting (EH) has attracted increasing interests, owing to its capability of converting received RF signals into electricity, which is able to provide stable and controllable power to prolong the lifetime of low-power energy-constrained networks, such as Internet of Things (IoT), wireless sensor networks (WSNs), wireless personal area networks (WPANs) and wireless body area networks (WBANs) [1]–[4]. It was reported that with current available EH circuits, microwatts to milliwatts of power can be harvested from received RF signals over the range of several meters with a transmit power of 1 Watt and a carrier frequency less than 1 GHz [4].

One important application of RF-EH is simultaneous wireless information and power transfer (SWIPT), where the same RF signal is used to transfer both energy and information, which potentially offers great possibility to replenish power and transmit information to energy-constrained devices (e.g., low-power sensor nodes) [5]–[10]. In [5], the single-input single-output (SISO) channel was considered, where a capacity-energy function was proposed to characterize the fundamental tradeoffs of SWIPT. It was shown that there exist a nontrivial tradeoff in maximizing information rate versus power transfer since the quantity of information contained in the RF signal is determined by the amount of "variations", i.e., entropy rate, while its carried power is determined by the average squared value of the amplitude. In [6], this tradeoff was further extended to frequency-selective channels. Zhang and Ho [7] investigated the information-energy tradeoff of SWIPT over a three-node multiple-input-multiple-output (MIMO) broadcasting channel in terms of *rate-energy (R-E) region*. In their work, two scenarios were examined, i.e., the *separated* information decoding (ID) and EH receivers scenario where the EH and ID receivers have different MIMO channels from the transmitter, and the *co-located* EH and ID receivers scenario where the EH and ID receivers have identical MIMO channels from the transmitter. Zhang and Ho [7] also pointed out that it is impractical for EH and ID receivers to receive information and collect energy using the same circuit as the EH and ID receivers have very different power sensitivities and the EH operation performed in the RF domain destroys the information content. Therefore, two practical receiver architectures (i.e., *time switching* (TS) and *power splitting* (PS)) were proposed in [7] for the co-located receivers scenario. So far, SWIPT has become an appealing EH technique and been applied to various wireless communication networks [8]–[18]. For example, in [25]–[27], multiuser MISO broadcast SWIPT systems were investigated, where the weighted sum-power transferred to all EH receivers was maximized in [25], the total transmission power at BS was minimized [26], and the capacity region for ID receivers was explored [27], respectively.

However, in all works mentioned above, *the linear EH model* was adopted, where the power conversion efficiency

Manuscript received July 28, 2016; revised November 12, 2016 and March 21, 2017; accepted May 14, 2017. Date of publication May 26, 2017; date of current version August 10, 2017. This work was supported in part by the National Natural Science Foundation of China under Grant 61671051, in part by the Beijing Natural Science Foundation of China under Grant 4162049, in part by the Open Research Fund of National Mobile Communications Research Laboratory, Southeast University, under Grant 2014D03, and in part by the Fundamental Research Funds for the Central Universities of Beijing Jiaotong University under Grant 2016JBM015. The associate editor coordinating the review of this paper and approving it for publication was W. H. Mow. *(Corresponding author: Ke Xiong.)*

K. Xiong is with the School of Computer and Information Technology, Beijing Jiaotong University, Beijing 100044, China, and also with the National Mobile Communications Research Laboratory, Southeast University, Nanjing 210018, China (e-mail: kxiong@bjtu.edu.cn).

B. Wang and K. J. R. Liu are with the Department of Electrical and Computer Engineering, University of Maryland at College Park, MD 20742 USA (e-mail: bebewang@umd.edu; kjrliu@umd.edu).

Color versions of one or more of the figures in this paper are available online at http://ieeexplore.ieee.org.

Digital Object Identifier 10.1109/TWC.2017.2706277

of the RF-EH circuit, defined as the ratio of the output direct currency (DC) power to the input RF signal power, was considered to be constant. That is, the output DC power was assumed to be independent of the input power level of the EH circuit. Recently, by measurement with real RF-EH circuit data, the authors in [28] found that in practical systems, RF-EH circuits usually show a nonlinear end-to-end RF-EH behavior rather than the linear one. Therefore, using the linear EH model in SWIPT system design may result in the mismatch and system performance degradation. To accurately capture the property of practical RF-EH circuits, [28] presented a *nonlinear EH model* based on the logistic function and real data. With the nonlinear EH model, [28] and [29] studied the resource allocation for multi-user SWIPT systems. It was shown that a substantial performance gain could be achieved when the resource allocation is performed with the nonlinear EH model instead of traditional linear EH model. Most recently, a few works began to study SWIPT systems with the nonlinear EH model, such as robust beamforming design [30], wireless power transfer efficiency maximization [31] and system outage analysis [32], [33].

As the nonlinear EH model is more practical and more accurate, in this paper, we focus on examining the performance limits of SWIPT MIMO broadcasting channel under the nonlinear EH model. In our work, the R-E region is adopted as the system performance index, as it is effective to characterize the tradeoff between the information and energy transfer, which may provide some fundamental and useful references in optimally designing SWIPT-enabled systems [9]. Similar to [7], two scenarios, i.e., the *separated* and the *co-located* EH and ID receivers scenarios, are considered. For the co-located EH and ID receivers scenario, both TS and PS receiver architectures are investigated.

The contributions of the paper are summarized as follows.

Firstly, for the two MIMO scenarios with PS and TS receiver architectures, we derive the boundaries of their R-E regions, where some optimization problems on maximizing the harvested energy are studied under a given information rate threshold with the nonlinear EH model constraint. Since the problems are non-convex and cannot be directly solved by using known solution methods, we propose efficient methods to solve them. We prove that the nonlinear EH model is a mathematically increasing function w.r.t. the received RF signal power. Therefore, the optimal solution of the nonlinear EH model system may have a similar structure with that of the linear EH model system in [7].

It is by no means that the optimal solution of the nonlinear EH model system can be directly derived by plugging the analytical result of the nonlinear system in the solution structure of the linear EH system. The reason is explained as follows. In [7], the R-E boundaries of the linear EH systems were obtained by solving some optimization problems, in which the information rate was maximized under the harvested energy constraint. In linear EH model case, these problems are convex and can be easily solved. But in nonlinear EH model case, they are non-convex due to the nonlinear EH constraints, resulting in the difficulty to solve them. As an alternative, we consider the maximization problems, in which the harvested energy is maximized under the constraint of information rate, to draw the boundaries of the R-E regions for the nonlinear EH systems. By doing so, we can obtain some semi-closed results on the optimal solutions and then design efficient solution algorithms. Therefore, both the considered problems and the solution methods are different from those in [7].

Secondly, we also obtain some new results on the nonlinear EH system design compared with [7]. For example, for the TS system with the linear EH model, Zhang and Ho [7] found that the minimal consumed power at the transmitter for the EH receiver to harvest power is independent of the time switching factor. In contrast, for the TS system with the nonlinear EH model, we found that the minimal consumed power at the transmitter for the EH receiver to harvest power is closely dependent on the time switching factor. Thus, we design new solution method for the TS MIMO broadcasting system with the nonlinear EH model and our obtained results are very different from those of the linear EH model in [7]. Besides, for the PS system with the linear EH model, the optimal power splitting factors were searched with a small step size over the interval $[0, 1]$ in [7], which may be too computationally complex for the system with a relatively large number of antennas. While, for the PS system with the nonlinear EH model, we find the optimal power splitting factors by solving a convex problem and derive a semi-closed form expression for them, which is with low complexity.

Thirdly, numerical results with different circuit parameter configurations are provided to evaluate the system performance under the nonlinear EH model, which provides some interesting insights on the SWIPT MIMO broadcasting channel. It is shown that all practical circuit specifications greatly affect the system R-E region. Compared with the systems under current linear EH model, the ones under the practical nonlinear EH model achieve smaller R-E regions and show different R-E tradeoff behaviors. Particularly, with the increment of R, the average maximum harvested energy in the separated EH and ID receivers system and in the PS system with the nonlinear EH model decreases with an increasing declining rate, but decreases with an almost constant declining rate in the TS system with the nonlinear EH model. Additionally, the PS system achieves larger average R-E region than the TS one under the nonlinear EH model.

The rest of the paper is organized as follows. Section II describes the system model. Section III and Section IV investigate the R-E regions for the separated receivers scenario and the co-located receivers scenario, respectively, by formulating and solving corresponding optimization problems. Section V provides some simulation results and finally Section VI concludes the paper.

Notations: $\mathbb{C}^{M\times N}$, $\mathbb{H}^{M\times N}$, $\mathbb{R}^{M\times N}$ denote the set of complex, Hermitian and real matrices with size of M rows and N columns, respectively. $E(\cdot)$ represents the expectation operator. $\|\cdot\|$ denotes the Frobenius norm. $\mathrm{Tr}(\mathbf{X})$ is the trace of matrix $\mathbf{X}$. $\mathbf{I}$ denotes an identity matrix and $\mathbf{0}$ denotes a zero matrix with all entries equaling to zero. $[x]^+$ is the operator which is defined as $[x]^+ = \max\{0, x\}$. $\preceq_{\mathbb{R}_+^M}$ denotes the generalized inequality defined over a set of non-negative

$M \times M$ matrices. $\mathbf{X} \succeq \mathbf{0}$ indicates that $\mathbf{X}$ is a positive semidefinite (PSD) matrix.

II. System Model

We consider a MIMO broadcasting network consisting of one transmitter, one EH receiver and one ID receiver, where all nodes are equipped with multiple antennas and the numbers of antennas at the transmitter, the EH and the ID receivers are denoted by N_{T}, N_{E} and N_{I}, respectively. Let $\mathbf{H}_{\mathrm{E}} \in \mathbb{C}^{N_{\mathrm{E}} \times N_{\mathrm{T}}}$ and $\mathbf{H}_{\mathrm{I}} \in \mathbb{C}^{N_{\mathrm{I}} \times N_{\mathrm{T}}}$ be the channel matrices between the transmitter and the EH receiver and between the transmitter and the ID receiver, respectively. Quasi-static fading channel is assumed at each fading state. Both $\mathbf{H}_{\mathrm{E}}$ and $\mathbf{H}_{\mathrm{I}}$ are known at the transmitter and the corresponding receivers so that energy beamforming or information precoding can be performed at the transmitter to enhance the system performance.

Denote $\mathbf{s}(k) \in \mathbb{C}^{N_{\mathrm{T}} \times 1}$ as the baseband signal broadcast by the transmitter at the k-th symbol interval. Without loss of generality, $\mathbf{s}(k)$ is assumed to be random over k. $\mathbf{Q} = E[\mathbf{s}(k)\mathbf{s}(k)^H]$ is the covariance matrix of $\mathbf{s}(k)$ satisfying that $E[\|\mathbf{s}(k)\|^2] = \mathrm{Tr}(\mathbf{Q}) \leq P$, where P is the average available power at the transmitter over all transmit antennas. Therefore, the received signal at the EH and ID receivers can be respectively given by $\mathbf{y}_{\mathrm{E}}(k) = \mathbf{H}_{\mathrm{E}}\mathbf{s}(k) + \mathbf{n}_{\mathrm{E}}(k)$ and $\mathbf{y}_{\mathrm{I}}(k) = \mathbf{H}_{\mathrm{I}}\mathbf{s}(k) + \mathbf{n}_{\mathrm{I}}(k)$, where $\mathbf{n}_{\mathrm{E}}(k) \in \mathbb{C}^{N_{\mathrm{E}} \times 1} \sim \mathcal{CN}(\mathbf{0}, \sigma_{\mathrm{E}}^2\mathbf{I})$ and $\mathbf{n}_{\mathrm{I}}(k) \in \mathbb{C}^{N_{\mathrm{I}} \times 1} \sim \mathcal{CN}(\mathbf{0}, \sigma_{\mathrm{I}}^2\mathbf{I})$ are the noise received at the EH and ID receivers, respectively. For the EH receiver, the input power is $E[\|\mathbf{H}_{\mathrm{E}}\mathbf{s}(k)\|^2] = \mathrm{Tr}(\mathbf{H}_{\mathrm{E}}\mathbf{Q}\mathbf{H}_{\mathrm{E}}^H)$. With the traditional linear EH model, the harvested energy at the EH receiver is given by

$$E_{\mathrm{linear}} = \eta E[\|\mathbf{H}_{\mathrm{E}}\mathbf{s}(k)\|^2] = \eta \mathrm{Tr}(\mathbf{H}_{\mathrm{E}}\mathbf{Q}\mathbf{H}_{\mathrm{E}}^H), \tag{1}$$

where $\eta \in (0, 1]$ is a constant, denoting the energy conversion efficiency and it is independent of the input power level at the EH receiver.

More recently, [28] found that the practical EH circuit results in a nonlinear end-to-end wireless power transfer so that they presented a nonlinear EH model based on the measurement data of practical EH circuits, which is more accurate to describe the characteristics of EH circuits. With the nonlinear EH model [28], [34], the harvested energy at the EH receiver can be given by

$$\begin{aligned} E_{\mathrm{nonlinear}} &= \frac{\frac{M}{1+\exp\left(-a(\mathrm{Tr}(\mathbf{H}_{\mathrm{E}}\mathbf{Q}\mathbf{H}_{\mathrm{E}}^H)-b)\right)} - \frac{M}{1+\exp(ab)}}{1 - \frac{1}{1+\exp(ab)}} \\ &\triangleq \Psi\left(\mathrm{Tr}(\mathbf{H}_{\mathrm{E}}\mathbf{Q}\mathbf{H}_{\mathrm{E}}^H)\right). \end{aligned} \tag{2}$$

In (2), $\Psi(x)$ is defined as a function of x, i.e., $\Psi(x) = \frac{\beta(x) - M\Omega}{1-\Omega}$, where $\Omega = \frac{1}{1+\exp(ab)}$ and $\beta(x) = \frac{M}{1+\exp(-a(x-b))}$ which is the traditional logistic function w.r.t. x. M is a constant, indicating the maximum harvested power at EH receiver when the EH circuit is saturated. Parameters a and b are constants depending on the detailed circuit specifications, such as resistance, capacitance and diode turn-on voltage. In practice, a, b, and M can be easily found by a standard curve fitting tool. Such a nonlinear EH model is capable of capturing the joint effect of the nonlinear phenomena induced by hardware constraints, e.g., circuit sensitivity limitations and current leakage [28].

It can be seen in (1) that with the linear EH model, the harvested energy can be increased with the increment of input power without limitation, while in (2), it was shown that with the nonlinear model, when the input power is relatively low, the harvested energy is increased with the increment of input power and the increasing rate is closely dependent on the parameters a and b. Moreover, there is a limitation on the maximum possible harvested energy for the nonlinear EH model. As the nonlinear EH model is more general and more accurate for practical EH systems, we shall investigate the MIMO broadcasting channel with it.

By observing (1) and (2), we obtain the following result.

Proposition 1: For the same $\boldsymbol{H_E}$ and $\boldsymbol{Q}$, the harvested energy of the nonlinear EH model over the MIMO broadcasting channel is bounded by that of the linear EH model with $\eta = 1$, i.e., $E_{nonlinear} \leq E_{linear}|_{\eta=1}$.

Proof: From (1), the harvested energy of the linear EH model is $\eta\mathrm{Tr}(\mathbf{H}_{\mathrm{E}}\mathbf{Q}\mathbf{H}_{\mathrm{E}}^H)$. From (2) of the nonlinear model, the input power is $\mathrm{Tr}(\mathbf{H}_{\mathrm{E}}\mathbf{Q}\mathbf{H}_{\mathrm{E}}^H)$ and the harvested energy is $E_{\mathrm{nonlinear}}$. Due to the law of conservation of energy, it is known that $E_{\mathrm{nonlinear}} \leq \mathrm{Tr}(\mathbf{H}_{\mathrm{E}}\mathbf{Q}\mathbf{H}_{\mathrm{E}}^H)$. That is $E_{\mathrm{nonlinear}} \leq E_{\mathrm{linear}}|_{\eta=1}$. ■

In such a system, for the ID receiver, its obtained information rate can be given by [35]

$$R = \log|\mathbf{I} + \tfrac{1}{\sigma_{\mathrm{I}}^2}\mathbf{H}_{\mathrm{I}}\mathbf{Q}\mathbf{H}_{\mathrm{I}}^H|. \tag{3}$$

It was proved in [7] that the maximal information delivering and power transfer are different from each other, which involve information spatial multiplexing and energy beamforming, respectively. Therefore, there is a tradeoff between them under given available power constraint, which can be described by the R-E region. Assuming the continuously transmitted signals from the transmitter is Gaussian signals, for example, the R-E region of MIMO channel with separated EH and ID receivers can be given by

$$\begin{aligned} \mathcal{C}_{\text{R-E}} \triangleq \Big\{ (R, E) \mid R \leq \log|\mathbf{I} + \tfrac{1}{\sigma_{\mathrm{I}}^2}\mathbf{H}_{\mathrm{I}}\mathbf{Q}\mathbf{H}_{\mathrm{I}}^H|, \\ E \leq \Psi\left(\mathrm{Tr}(\mathbf{H}_{\mathrm{E}}\mathbf{Q}\mathbf{H}_{\mathrm{E}}^H)\right), \mathrm{Tr}(\mathbf{Q}) \leq P, \mathbf{Q} \succeq \mathbf{0} \Big\}. \end{aligned} \tag{4}$$

As shown in Figure 1, there are two different scenarios for the MIMO broadcasting system. The first one is with separated EH and ID receivers, see Figure 1 (a), and the second one is with co-located EH and ID receivers, see Figure 1 (b). For the co-located EH and ID receivers scenario, two practical receiver architectures, i.e., TS and PS receiver architectures, were proposed in [7]. With TS architecture employed, the receiver switches in time domain between the EH and ID receivers and the entire signal received in one time slot is used either for ID or EH, as shown in Figure 1 (b). With PS architecture employed, the received signals are split into two streams of different power levels in terms of a PS factor, where one signal stream is sent to the rectenna circuit for EH and the other is converted to baseband for ID, as shown in Figure 1 (b)(2). Comparatively, the TS architecture allows for a simple hardware implementation at the receiver but requires accurate time

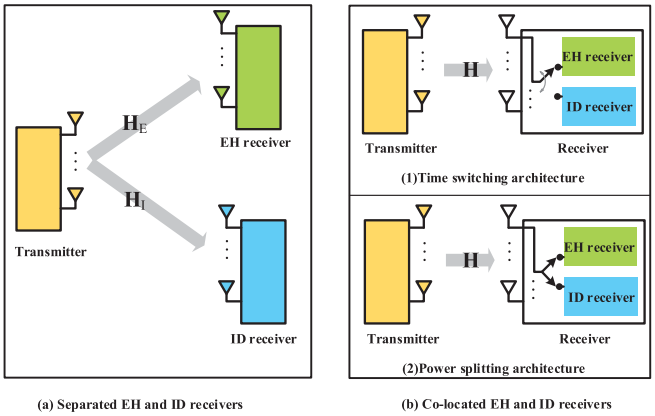

Fig. 1. System model: (a) Separated EH and ID receiver; (b) Co-located EH and ID receivers: (1) TS receiver architecture and (2)PS receiver architecture.

synchronization and information/energy scheduling while the PS architecture doesn't need accurate time synchronization and information/energy scheduling but requires a relatively complex hardware implementation.

In Section III and IV, we shall respectively discuss the R-E regions of the MIMO broadcasting system with separated receivers and co-located receivers, respectively.

III. R-E Region for Separated EH and ID Receivers

In this section, we consider the MIMO broadcasting system with separated EH and ID receivers, whose R-E region is described by (4). To figure out the R-E region, the four points on the region boundary, i.e., $(0, E_{\max})$, $(R_{\text{EH}}, E_{\max})$, $(R_{\max}, E_{\text{ID}})$ and $(R_{\max}, 0)$ on the R-E coordinate plane, should be determined at first.

A. Calculation of E_{max}

To find out $E_{\max}$, the case when the ID receiver is not present should be considered. In this case, the objective of the MIMO system design is to maximize the harvested energy E under the transmitter's power constraint, which can be express by

$$\mathbf{P}_1: \max_{\mathbf{Q}_\text{E}} E_{\text{nonlinear}} = \Psi\left(\text{Tr}(\mathbf{H}_\text{E}\mathbf{Q}_\text{E}\mathbf{H}_\text{E}^H)\right) \quad \text{s.t. } \text{Tr}(\mathbf{Q}_\text{E}) \le P,\ \mathbf{Q}_\text{E} \succeq \mathbf{0}, \tag{5}$$

where $\mathbf{Q}_\text{E}$ is the energy beamforming covariance matrix at the transmitter, which is required to be optimized. Although the two constraints in Problem $\mathbf{P}_1$ are convex sets, the objective function $\Psi\left(\text{Tr}(\mathbf{H}_\text{E}\mathbf{Q}_\text{E}\mathbf{H}_\text{E}^H)\right)$ is neither convex nor concave w.r.t $\mathbf{Q}_\text{E}$. So, it cannot be directly solved by using standard solution method for convex problems. However, fortunately, we found the following property of the objective function.

Lemma 1: *$\Psi(x)$ is a monotonically increasing function w.r.t x.*

Proof: Suppose $x_1 > x_2 > 0$. It can be easily proved that $\Psi(x_1) - \Psi(x_2) > 0$ always holds by some simple algebraic operations. Therefore, Lemma 1 is proved. ■

Lemma 1 indicates the following two facts:

Fact 1: $E_{\text{nonlinear}} = \Psi\left(\text{Tr}(\mathbf{H}_\text{E}\mathbf{Q}_\text{E}\mathbf{H}_\text{E}^H)\right)$ is an injective function w.r.t $\text{Tr}(\mathbf{H}_\text{E}\mathbf{Q}_\text{E}\mathbf{H}_\text{E}^H)$, vise versa;

Fact 2: A larger $\text{Tr}(\mathbf{H}_\text{E}\mathbf{Q}_\text{E}\mathbf{H}_\text{E}^H)$ yields a higher $E_{\text{nonlinear}}$.

Lemma 2: Suppose $f(x)$ is a concave function and $F(f(x))$ is a monotonically increasing function of $f(x)$, then the two optimization problems, i.e., $\max_x f(x)$ subject to $C_1(x), C_2(x), \ldots, C_m(x)$ and $\max_x F(f(x))$ subject to $C_1(x), C_2(x), \ldots, C_m(x)$ have the same optimal solution (but usually different optimal values of the objective functions), where $C_i(x)$ is a convex set for all $i = 1, \ldots, m$.

Proof: Since the two problems have the same constraints, they have the same feasible solution sets. Moreover, as $f(x)$ is concave, there exists a unique optimal solution x^* for problem $\max_x f(x)$ subject to $C_1(x)$, $C_2(x)$, …, $C_m(x)$ such that $f(x^*)$ achieves the maximum. Suppose there exists another $x^\sharp$ satisfying that $\beta(f(x^\sharp)) > F(f(x^*))$. As $\beta(f(x))$ is a monotonically increasing function of $f(x)$, it indicates that $f(x^\sharp) > f(x^*)$, which contradicts that x^* is the optimal solution of $\max_x f(x)$. Therefore, such a $x^\sharp$ does not exist, which implies that $F(f(x^*))$ achieves its maximum, i.e., x^* is also the optimal solution of the optimization problem $F(f(x))$ subject to $C_1(x)$, $C_2(x)$, …, $C_m(x)$. ■

According to Lemma 1 and Lemma 2, it can be deduced that Problem $\mathbf{P}_1$ has the same solution of the following Problem $\mathbf{P}_1'$, i.e.,

$$\mathbf{P}_1': \max_{\mathbf{Q}_\text{E}} \text{Tr}(\mathbf{H}_\text{E}\mathbf{Q}_\text{E}\mathbf{H}_\text{E}^H) \quad \text{s.t. } \text{Tr}(\mathbf{Q}_\text{E}) \le P, \quad \mathbf{Q}_\text{E} \succeq \mathbf{0}. \tag{6}$$

It means that once the optimal $\mathbf{Q}_\text{E}^*$ of Problem $\mathbf{P}_1'$ is found, by substituting it into the objective function of Problem $\mathbf{P}_1$, one can obtain $E_{\max}$. Since Problem $\mathbf{P}_1'$ has the similar form to the problem $\mathbf{P}_1$ in [7], the optimal solution of Problem $\mathbf{P}_1'$ can be accordingly given by

$$\mathbf{Q}_\text{E}^* = P\boldsymbol{v}_\text{E}^{(1)}(\boldsymbol{v}_\text{E}^{(1)})^H, \tag{7}$$

where $\boldsymbol{v}_\text{E}^{(1)}$ is the first column of V_E. $V_\text{E} \in \mathbb{C}^{N_\text{T}\times\min\{N_\text{T},N_\text{E}\}}$ is obtained by the singular value decomposition (SVD) of channel matrix $\mathbf{H}_\text{E}$, i.e., $\mathbf{H}_\text{E} = \mathbf{U}_\text{E}\mathbf{\Sigma}_\text{E}\mathbf{V}_\text{E}^H$, where $\mathbf{\Sigma}_\text{E} = \text{diag}\left(\sqrt{h_1^{(\text{e})}}, \sqrt{h_2^{(\text{e})}}, \ldots, \sqrt{h_{\min\{N_\text{T},N_\text{E}\}}^{(\text{e})}}\right)$ with $h_1^{(\text{e})} \ge h_2^{(\text{e})} \ge \ldots \ge h_{\min\{N_\text{T},N_\text{E}\}}^{(\text{e})} \ge 0$. $\mathbf{U}_\text{E} \in \mathbb{C}^{N_\text{E}\times\min\{N_\text{T},N_\text{E}\}}$ and $\mathbf{V}_\text{E} \in \mathbb{C}^{N_\text{T}\times\min\{N_\text{T},N_\text{E}\}}$, each of which consists orthogonal columns with unit norm. Consequently,

$$E_{\max} = \Psi(h_1^{(\text{e})}P). \tag{8}$$

B. Calculation of R_{max}

To find out $R_{\max}$, the case when the EH receiver is not present should be considered. In this case, the objective of the MIMO system design is to maximize the received information R under the transmitter's power constraint, which can be expressed by

$$\mathbf{P}_2: \max_{\mathbf{Q}_\text{I}} R = \log|\mathbf{I} + \tfrac{1}{\sigma_\text{I}^2}\mathbf{H}_\text{I}\mathbf{Q}_\text{I}\mathbf{H}_\text{I}^H| \quad \text{s.t. } \text{Tr}(\mathbf{Q}_\text{I}) \le P, \quad \mathbf{Q}_\text{I} \succeq \mathbf{0}, \tag{9}$$

where $\mathbf{Q}_\text{I}$ is the information precoding covariance matrix at the transmitter, which is required to be optimized.

According to [35], the optimal solution follows the following structure, i.e.,

$$\mathbf{Q}_{\mathrm{I}}^{*} = \mathbf{V}_{\mathrm{I}}\mathbf{\Lambda}_{\mathrm{S_I}}\mathbf{V}_{\mathrm{I}}^{H}, \tag{10}$$

where $\mathbf{V}_{\mathrm{I}} \in \mathbb{C}^{N_{\mathrm{T}}\times\min\{N_{\mathrm{T}},N_{\mathrm{I}}\}}$ is obtained by the SVD of channel matrix $\mathbf{H}_{\mathrm{I}}$, i.e., $\mathbf{H}_{\mathrm{I}} = \mathbf{U}_{\mathrm{I}}\mathbf{\Sigma}_{\mathrm{I}}\mathbf{V}_{\mathrm{I}}^{H}$ and $\mathbf{\Sigma}_{\mathrm{I}} = \mathrm{diag}\left(\sqrt{h_1^{(\mathrm{I})}}, \sqrt{h_2^{(\mathrm{I})}}, \ldots, \sqrt{h_{\min\{N_{\mathrm{T}},N_{\mathrm{I}}\}}^{(\mathrm{I})}}\right)$ with $h_1^{(\mathrm{I})} \geq h_2^{(\mathrm{I})} \geq \ldots \geq h_{\min\{N_{\mathrm{T}},N_{\mathrm{I}}\}}^{(\mathrm{I})} \geq 0$. $\mathbf{\Lambda}_{\mathrm{S_I}} = \mathrm{diag}(p_1, p_2, \ldots, p_{\min\{N_{\mathrm{T}},N_{\mathrm{I}}\}})$ with the elements derived from standard water-filling power allocation [35], i.e., $p_i = \left[\nu - \frac{1}{h_i^{(\mathrm{I})}}\right]^{+}, \forall i = 1, 2, \ldots, \min\{N_{\mathrm{T}}, N_{\mathrm{I}}\}$, where ν is a positive constant (the water-level contant) such that $\sum_{i=1}^{\min\{N_{\mathrm{T}},N_{\mathrm{I}}\}} p_i = P$. As a result, the corresponding maximum information rate can be given by

$$R_{\max} = \sum\nolimits_{i=1}^{\min\{N_{\mathrm{T}},N_{\mathrm{I}}\}} \log\left(1 + \frac{p_i h_i^{(\mathrm{I})}}{\sigma_{\mathrm{I}}^2}\right). \tag{11}$$

Now, with the obtained $E_{\max}$ and $R_{\max}$ above, the other two boundary points i.e., $(R_{\mathrm{EH}}, E_{\max})$ and $(R_{\max}, E_{\mathrm{ID}})$ of the R-E region can be obtained. We consider the case where EH and ID receivers are co-exist to determine R_{EH} and E_{ID}. Specifically, R_{EH} is the achieved information rate at the ID receiver when the transmitter adopts the optimal precoding matrix in (7) to achieve $E_{\max}$ at the EH receiver. Thus, we have $R_{\mathrm{EH}} = \log\left(1 + \frac{P}{\sigma_{\mathrm{I}}^2}\|\mathbf{H}_{\mathrm{I}}\boldsymbol{v}_{\mathrm{E}}^{(1)}\|^2\right)$. E_{ID} is the harvested energy at the EH receiver when the transmitter adopts the optimal beam matrix in (10) to achieve $R_{\max}$ at the ID receiver and it can be given by $E_{\mathrm{ID}} = \Psi\left(\mathrm{Tr}(\mathbf{V}_{\mathrm{I}}\mathbf{\Lambda}_{\mathrm{S_I}}\mathbf{V}_{\mathrm{I}}^{H})\right)$.

C. R-E Region of the Separated EH and ID Receivers System

When $R \leq R_{\mathrm{EH}}$, $E_{\max}$ is achievable at the EH receiver with the transmit covariance matrix in (7) adopted at the transmitter. When $E \leq E_{\mathrm{ID}}$, $R_{\max}$ is achievable at the ID receiver with the transmit covariance matrix in (10) adopted at the transmitter. Therefore, it only needs to determine the boundary of $\mathcal{C}_{\text{R-E}}$ over the intervals $R_{\mathrm{EH}} \leq R \leq R_{\max}$ and $E_{\mathrm{ID}} \leq E \leq E_{\max}$ on the R-E plane. To do so, either of the following optimization problems can be considered, i.e.,

$$\begin{aligned}\mathbf{P}_3\colon \quad & \max_{\mathbf{Q}} \ R = \log|\,\mathbf{I} + \tfrac{1}{\sigma_{\mathrm{I}}^2}\mathbf{H}_{\mathrm{I}}\mathbf{Q}\mathbf{H}_{\mathrm{I}}^{H}\,| \\ & \text{s.t. } \Psi\left(\mathrm{Tr}(\mathbf{H}_{\mathrm{E}}\mathbf{Q}\mathbf{H}_{\mathrm{E}}^{H})\right) \geq E, \quad \mathrm{Tr}(\mathbf{Q}) \leq P, \quad \mathbf{Q}\succeq \mathbf{0},\end{aligned} \tag{12}$$

where E takes values from E_{ID} to $E_{\max}$, or

$$\begin{aligned}\mathbf{P}_4\colon \quad & \max_{\mathbf{Q}} \ E_{\mathrm{nonlinear}} = \Psi\left(\mathrm{Tr}(\mathbf{H}_{\mathrm{E}}\mathbf{Q}\mathbf{H}_{\mathrm{E}}^{H})\right) \\ & \text{s.t. } \log|\,\mathbf{I} + \tfrac{1}{\sigma_{\mathrm{I}}^2}\mathbf{H}_{\mathrm{I}}\mathbf{Q}\mathbf{H}_{\mathrm{I}}^{H}\,| \geq R, \quad \mathrm{Tr}(\mathbf{Q}) \leq P, \quad \mathbf{Q}\succeq \mathbf{0},\end{aligned} \tag{13}$$

where R takes values from R_{EH} to $R_{\max}$. It is observed that in Problem $\mathbf{P}_3$, the objective function is concave, but the constraint, $\Psi\left(\mathrm{Tr}(\mathbf{H}_{\mathrm{E}}\mathbf{Q}\mathbf{H}_{\mathrm{E}}^{H})\right) \geq E$, is a non-convex set. In Problem $\mathbf{P}_4$, all the constraints are convex sets but the objective function is neither convex nor concave. Hence, both Problem $\mathbf{P}_3$ and Problem $\mathbf{P}_4$ are non-convex and cannot be directly solved. However, we found that by solving the following Problem $\mathbf{P}_4'$, one can obtain the same solution to Problem $\mathbf{P}_4$.

$$\begin{aligned}\mathbf{P}_4'\colon \quad & \max_{\mathbf{Q}} \ \mathrm{Tr}(\mathbf{H}_{\mathrm{E}}\mathbf{Q}\mathbf{H}_{\mathrm{E}}^{H}) \\ & \text{s.t. } \log|\,\mathbf{I} + \tfrac{1}{\sigma_{\mathrm{I}}^2}\mathbf{H}_{\mathrm{I}}\mathbf{Q}\mathbf{H}_{\mathrm{I}}^{H}\,| \geq R, \quad \mathrm{Tr}(\mathbf{Q}) \leq P, \quad \mathbf{Q}\succeq \mathbf{0},\end{aligned} \tag{14}$$

which is a convex problem.

Lemma 3: Problem $\boldsymbol{P}_4'$ has the same optimal solution with Problem $\boldsymbol{P}_4$.

Proof: One can see that the constraint sets of both Problem $\mathbf{P}_4$ and Problem $\mathbf{P}_4'$ are the same. According to Fact 1, Lemma 1 and Lemma 2, it can be easily proved that Problem $\mathbf{P}_4$ has the same optimal solution with Problem $\mathbf{P}_4'$. ∎

Therefore, we consider Problem $\mathbf{P}_4$ and Problem $\mathbf{P}_4'$ to determine the boundary of the R-E region for MIMO broadcasting with separated EH and ID receivers.[1] The Lagrangian of Problem $\mathbf{P}_4'$ can be given by

$$\begin{aligned}&\mathscr{L}(\mathbf{Q}, \mu, \nu) \\ &\quad = \mathrm{Tr}(\mathbf{H}_{\mathrm{E}}\mathbf{Q}\mathbf{H}_{\mathrm{E}}^{H}) + \mu\left(\log|\,\mathbf{I} + \tfrac{1}{\sigma_{\mathrm{I}}^2}\mathbf{H}_{\mathrm{I}}\mathbf{Q}\mathbf{H}_{\mathrm{I}}^{H}\,| - R\right) \\ &\qquad + \nu\left(P - \mathrm{Tr}(\mathbf{Q})\right) \\ &\quad = \mathrm{Tr}\left((\mathbf{H}_{\mathrm{E}}^{H}\mathbf{H}_{\mathrm{E}} - \nu\mathbf{I})\mathbf{Q}\right) + \mu\log|\,\mathbf{I} + \tfrac{1}{\sigma_{\mathrm{I}}^2}\mathbf{H}_{\mathrm{I}}\mathbf{Q}\mathbf{H}_{\mathrm{I}}^{H}\,| \\ &\qquad + \nu P - \mu R,\end{aligned} \tag{15}$$

where μ and ν are non-negative Lagrangian multipliers. Then, the Lagrangian dual function of Problem $\mathbf{P}_4'$ is defined as

$$\mathscr{G} = \max_{\mathbf{Q}\succeq 0} \ \mathscr{L}(\mathbf{Q}, \mu, \nu) \tag{16}$$

and the dual problem of Problem $\mathbf{P}_4'$ is

$$\min \ \mathscr{G}(\mu, \nu) \ \text{ s.t. } \ \mu \geq 0, \nu \geq 0. \tag{17}$$

Lemma 4: The Lagrangian multiplier ν in (15) satisfies that $\nu > \lambda_1$, where λ_1 is obtained by performing SVD on matrix $\boldsymbol{H_I B^{-\frac{1}{2}}}$, i.e., $\boldsymbol{H_I B^{-\frac{1}{2}}} = \hat{\boldsymbol{U}}\boldsymbol{\Lambda}_{\mathrm{H_I B}}\hat{\boldsymbol{V}}^{H}$. $\boldsymbol{\Lambda}_{\mathrm{H_I B}} = diag\left(\sqrt{\lambda_1}, \sqrt{\lambda_2}, \ldots, \sqrt{\lambda_{\min\{N_T,N_I\}}}\right)$ with $\lambda_1 \geq \lambda_2 \geq \ldots \geq \lambda_{\min\{N_T,N_I\}} \geq 0$ and $\boldsymbol{B} \triangleq \nu\boldsymbol{I} - \boldsymbol{H}_E^{H}\boldsymbol{H}_E$.

Proof: The proof of Lemma 4 can be found in Appendix A. ∎

Theorem 1: For given $\nu > \lambda_1$, the optimal solution of (16) is

$$\mathbf{Q}^{\sharp} = \mathbf{B}^{-\frac{1}{2}}\hat{\mathbf{V}}\mathbf{\Lambda}_{\mathrm{F}}\hat{\mathbf{V}}^{H}\mathbf{B}^{-\frac{1}{2}}, \tag{18}$$

where $\hat{\mathbf{V}}$ is obtained by performing SVD on matrix $\mathbf{H_I B^{-\frac{1}{2}}}$,

[1] Note that for the linear EH model case, the energy constraint $\Psi\left(\mathrm{Tr}(\mathbf{H}_{\mathrm{E}}\mathbf{Q}\mathbf{H}_{\mathrm{E}}^{H})\right) \geq E$ reduces to $\mathrm{Tr}(\mathbf{H}_{\mathrm{E}}\mathbf{Q}\mathbf{H}_{\mathrm{E}}^{H}) \geq \Psi^{-1}(E)$, which is a convex set. So, Problem $\mathbf{P}_3$ in the linear EH case is a convex problem. Therefore, in [7], Problem $\mathbf{P}_3$ was considered to drive the R-E region of linear EH model system rather than Problem $\mathbf{P}_4$.

i.e., $\mathbf{H}_{\mathrm{I}}\mathbf{B}^{-\frac{1}{2}} = \hat{\mathbf{U}}\mathbf{\Lambda}_{\mathrm{H_I B}}\hat{\mathbf{V}}^H$ *and*

$$\mathbf{\Lambda}_{\mathrm{F}} = \mathrm{diag}\Bigg(\left(\frac{\mu}{\sigma_{\mathrm{I}}^{2N_{\mathrm{I}}}\ln 2} - \frac{1}{\lambda_1}\right)^+, \left(\frac{\mu}{\sigma_{\mathrm{I}}^{2N_{\mathrm{I}}}\ln 2} - \frac{1}{\lambda_2}\right)^+, \ldots, \left(\frac{\mu}{\sigma_{\mathrm{I}}^{2N_{\mathrm{I}}}\ln 2} - \frac{1}{\lambda_{\min\{N_{\mathrm{T}},N_{\mathrm{I}}\}}}\right)^+\Bigg). \tag{19}$$

and μ should be selected to meet the constraint $Tr(\boldsymbol{Q}^\sharp) = P$.

Proof: The proof of Theorem 1 can be found in Appendix B. ∎

Now, we begin to solve the dual problem (17) by adopting the sub-gradient method, which can be described by Algorithm 1, where current optimal $\mathbf{Q}^*$ is calculated according to (18) with the given $\mu^{(n)}$ and $\nu^{(n)}$ and then the sub-gradient of $\mathscr{G}(\mu, \nu)$ is calculated and $\mu^{(n)}$ and $\nu^{(n)}$ are updated with an appropriate step size of the n-th iteration, $\varrho^{(n)}$.[2] When $\mu^{(n)}$ and $\nu^{(n)}$ converge to the pre-defined precision ϵ, the global optimal μ^* and ν^* are obtained. Substituting them into (18), the global optimal $\mathbf{Q}^*$, i.e. the optimal solution of Problem $\mathbf{P}_4'$ and $\mathbf{P}_4$, can be derived. Note that as Problem $\mathbf{P}_4$ is a convex problem, the duality gap between it and its dual problem is zero, which means the global optimal solution is guaranteed.

Algorithm 1 Calculate the Optimal $\mathbf{Q}^*$

1: **Initialization**:
   Set $\nu^{(0)} > \lambda_1$, $\mu^{(0)} \geq 0$;
   Calculate $\mathbf{Q}^\sharp$ according to (18) with the given $\nu^{(0)}$;
   Calculate $\mu^{(1)} = \left[\mu^{(0)} - \varrho^{(0)}\big(\log \mid \mathbf{I} + \frac{1}{\sigma^2}\mathbf{H}_{\mathrm{I}}\mathbf{Q}^\sharp\mathbf{H}_{\mathrm{I}}^H \mid - R\big)\right]^+$;
   Calculate $\nu^{(1)} = \left[\nu^{(0)} - \varrho^{(0)}\left(P - \mathrm{Tr}(\mathbf{Q})\right)\right]^+$;
   Set $n = 1$;
2: **Repeat**:
3: **while** $|\nu^{(n)} - \nu^{(n-1)}| > \epsilon$ or $|\mu^{(n)} - \mu^{(n-1)}| > \epsilon$ **do**
4: Calculate $\mathbf{Q}^\sharp$ according to (18) with the given $\nu^{(n)}$;
5: Update $\mu^{(n+1)} = \left[\mu^{(n)} - \varrho^{(n)}\big(\log \mid \mathbf{I} + \frac{1}{\sigma^2}\mathbf{H}_{\mathrm{I}}\mathbf{Q}^\sharp\mathbf{H}_{\mathrm{I}}^H \mid - R\big)\right]^+$;
   Update $\nu^{(n+1)} = \left[\nu^{(n)} - \varrho^{(n)}\big(P - \mathrm{Tr}(\mathbf{Q})\big)\right]^+$;
6: $n = n + 1$;
7: **end while**
8: Return $\mathbf{Q}^* = \mathbf{Q}^\sharp$.

Proposition 2: The R-E region of the MIMO broadcasting channel with separated EH and ID receiver under the nonlinear EH model is bounded by that under linear EH model with $\eta = 1$.

Proof: From Proposition 1, we know that the maximal harvested energy under the nonlinear EH model must be equal or lower than that the linear EH model with $\eta = 1$, i.e., $E_{\max}^{(\mathrm{nonlinear})} \leq E_{\max}^{(\mathrm{linear})}$. Moreover, the $R_{\max}^{(\mathrm{nonlinear})}$ in (11) is the same with that of the linear EH model, i.e., $R_{\max}^{(\mathrm{nonlinear})} = R_{\max}^{(\mathrm{linear})}$. This means that the four points, $(0, E_{\max})$, $(R_{\mathrm{EH}}, E_{\max})$, $(R_{\max}, E_{\mathrm{ID}})$ and $(R_{\max}, 0)$ on the region boundary of the nonlinear model is bounded by those of the linear model. Furthermore, since Problem $\mathbf{P}_4$ has the same optimal solution with Problem $\mathbf{P}_4'$, combining it with Proposition 1, it can be known that the optimal value of Problem $\mathbf{P}_4$ can not be larger than that of Problem $\mathbf{P}_4'$, which means that the boundary curve associated with the nonlinear model from R_{EH} to $R_{\max}$ is also bounded by that associated with the linear model with $\eta = 1$. As a result, Proposition 2 is arrived. ∎

[2]The value of $\varrho^{(n)}$ should be selected according to backtracking line search method [36] for achieving fast convergence.

IV. R-E Region of Co-Located EH and ID Receivers

When EH and ID receivers are co-located, $\mathbf{H}_{\mathrm{E}} = \mathbf{H}_{\mathrm{I}}$ and $N_{\mathrm{E}} = N_{\mathrm{I}}$. For convenience, we define $\mathbf{H} \triangleq \mathbf{H}_{\mathrm{E}} = \mathbf{H}_{\mathrm{I}}$ and $N \triangleq N_{\mathrm{E}} = N_{\mathrm{I}}$. To figure out the R-E region described by (4) for the co-located receiver case, the two points on the boundary of the R-E region should be determined at first, i.e., $(0, E_{\max})$ and $(R_{\max}, 0)$. It can be easily known that the results associated with $E_{\max}$ and $R_{\max}$ shown in (8) and (10) still hold for the co-located receiver case. Therefore, the boundary of the R-E region can be determined by considering following optimization problem,

$$\mathbf{P}_5: \quad \max_{\mathbf{Q}} \; E_{\mathrm{nonlinear}} = \Psi\left(\mathrm{Tr}(\mathbf{H}\mathbf{Q}\mathbf{H}^H)\right) \quad \text{s.t. } \log\mid \mathbf{I} + \tfrac{1}{\sigma^2}\mathbf{H}\mathbf{Q}\mathbf{H}^H \mid \geq R, \quad \mathrm{Tr}(\mathbf{Q}) \leq P, \; \mathbf{Q} \succeq \mathbf{0}, \tag{20}$$

where R takes values from 0 to $R_{\max}$.

A. Time Switching

With the time switching receiver architecture, the time switcher switches the signal input between the EH and ID receivers in time domain with a time switching factor θ, where $0 \leq \theta \leq 1$. Similar to [7], two types of power constraints can be considered for the TS system, i.e., fixed power and flexible power constraints. For fixed power constraint, its R-E region is expressed as

$$\mathcal{C}_{\text{R-E}}^{\mathrm{TS}_1} \triangleq \bigcup\nolimits_{0\leq\theta\leq 1}\Big\{(R, E) \mid E \leq \theta\Psi\left(\mathrm{Tr}(\mathbf{H}\mathbf{Q}_{\mathrm{E}}\mathbf{H}^H)\right), \; R \leq (1-\theta)\log|\mathbf{I} + \tfrac{1}{\sigma^2}\mathbf{H}\mathbf{Q}_{\mathrm{I}}\mathbf{H}^H|, \; \mathrm{Tr}(\mathbf{Q}_{\mathrm{E}}) \leq P, \quad \mathrm{Tr}(\mathbf{Q}_{\mathrm{I}}) \leq P, \; \mathbf{Q}_{\mathrm{E}}, \mathbf{Q}_{\mathrm{I}} \succeq \mathbf{0}\Big\}. \tag{21}$$

For flexible power constraint, its R-E region can be expressed as

$$\mathcal{C}_{\text{R-E}}^{\mathrm{TS}_2} \triangleq \bigcup\nolimits_{0\leq\theta\leq 1}\Big\{(R, E) \mid E \leq \theta\Psi\left(\mathrm{Tr}(\mathbf{H}\mathbf{Q}_{\mathrm{E}}\mathbf{H}^H)\right), \; R \leq (1-\theta)\log|\mathbf{I} + \tfrac{1}{\sigma^2}\mathbf{H}\mathbf{Q}_{\mathrm{I}}\mathbf{H}^H|, \; \theta\mathrm{Tr}(\mathbf{Q}_{\mathrm{E}}) + (1-\theta)\mathrm{Tr}(\mathbf{Q}_{\mathrm{I}}) \leq P, \mathbf{Q}_{\mathrm{E}}, \mathbf{Q}_{\mathrm{I}} \succeq \mathbf{0}\Big\}. \tag{22}$$

Since any pair of $(\mathbf{Q}_{\mathrm{E}} \succeq \mathbf{0}, \mathbf{Q}_{\mathrm{I}} \succeq \mathbf{0})$ satisfying the fixed power constraint always satisfy the flexible power constraint, the result $\mathcal{C}_{\text{R-E}}^{\mathrm{TS}_1} \subseteq \mathcal{C}_{\text{R-E}}^{\mathrm{TS}_2}$ obtained in [7] with under linear EH model also holds for the nonlinear EH model. Our goal is to explore the potential achievable R-E region of the MIMO broadcasting channel under the nonlinear EH model.

Therefore, in the following, we only focus on the boundary of $\mathcal{C}_{\text{R-E}}^{\text{TS}_2}$.

For a given θ, according to (8), the maximal energy can be harvested is $\theta\Psi(P_{\text{E}}h_1)$ when $\mathbf{Q}_{\text{E}} = P_{\text{E}}\boldsymbol{v}_{\text{H}}^{(1)}(\boldsymbol{v}_{\text{H}}^{(1)})^H$, where h_1 is obtained by the SVD of channel matrix $\mathbf{H}$. $\boldsymbol{v}_{\text{H}}^{(1)}$ is the eigenvector of the matrix $\mathbf{H}^H\mathbf{H}$ corresponding to the largest eigenvalue h_1 and P_{E} is the consumed transmit power for energy transfer. In order to harvest energy with amount of E, we can calculate the minimal consumed power by solving $E = \theta\Psi(P_{\text{E}}h_1)$. Since $\Psi^{-1}(x) = \frac{1}{a}\ln\left(\frac{\frac{x}{M}\exp(ab)+1}{\frac{x}{M}+1}\right)$, we have that $h_1\ P_{\text{E}} = \frac{1}{a}\ln\left(\frac{\frac{E/\theta}{M}\exp(ab)+1}{\frac{E/\theta}{M}+1}\right)$. As a result, the minimal consumed power at the transmitter for the EH receiver to harvest power E is given by

$$P_{\text{E}} = \frac{1}{ah_1}\ln\left(\frac{\frac{E/\theta}{M}\exp(ab)+1}{1+\frac{E/\theta}{M}}\right),$$

which depends on θ. This result is very different from that of the linear EH model case in [7], where the minimum consumed energy is independent of θ. Thus, the method proposed in [7] cannot be used to explore the R-E region of (22). Instead, we consider the following optimization problem to determine the boundary of $\mathcal{C}_{\text{R-E}}^{\text{TS}_2}$.

$$\begin{aligned}\mathbf{P}_6:\ \max_{\mathbf{Q}_{\text{E}},\mathbf{Q}_{\text{I}},\theta}\ & \theta\Psi\left(\text{Tr}(\mathbf{H}\mathbf{Q}_{\text{E}}\mathbf{H}^H)\right)\\ \text{s.t. }& (1-\theta)\log|\mathbf{I}+\tfrac{1}{\sigma^2}\mathbf{H}\mathbf{Q}_{\text{I}}\mathbf{H}^H|\geq R,\\ & \theta\text{Tr}(\mathbf{Q}_{\text{E}})+(1-\theta)\text{Tr}(\mathbf{Q}_{\text{I}})\leq P,\\ & \mathbf{Q}_{\text{E}},\ \mathbf{Q}_{\text{I}}\succeq\mathbf{0},\ 0\leq\theta\leq 1.\end{aligned}\tag{23}$$

It is observed that Problem $\mathbf{P}_6$ is not joint convex w.r.t $\mathbf{Q}_{\text{E}}$, $\mathbf{Q}_{\text{I}}$ and θ due to the coupling of them, so the optimal solution of the three variables cannot be jointly solved by using known convex optimization solution methods. Therefore, we solve it as follows.

1) Optimal $\boldsymbol{Q}_E^\sharp$ and $\boldsymbol{Q}_I^\sharp$ for Given θ: For a given θ, Problem $\mathbf{P}_6$ is reduced to

$$\begin{aligned}\max_{\mathbf{Q}_{\text{E}},\mathbf{Q}_{\text{I}}}\ & \theta\Psi\left(\text{Tr}(\mathbf{H}\mathbf{Q}_{\text{E}}\mathbf{H}^H)\right)\\ \text{s.t. }& (1-\theta)\log|\mathbf{I}+\tfrac{1}{\sigma^2}\mathbf{H}\mathbf{Q}_{\text{I}}\mathbf{H}^H|\geq R,\\ & \theta\text{Tr}(\mathbf{Q}_{\text{E}})+(1-\theta)\text{Tr}(\mathbf{Q}_{\text{I}})\leq P,\\ & \mathbf{Q}_{\text{E}}\succeq\mathbf{0},\quad \mathbf{Q}_{\text{I}}\succeq\mathbf{0},\end{aligned}\tag{24}$$

which is non-convex. Nevertheless, similar to Problem $\mathbf{P}_4$, we found that problem (24) has the same optimal solution with the following optimization problem, i.e.,

$$\begin{aligned}\max_{\mathbf{Q}_{\text{E}},\mathbf{Q}_{\text{I}}}\ & \text{Tr}(\mathbf{H}\mathbf{Q}_{\text{E}}\mathbf{H}^H)\\ \text{s.t. }& (1-\theta)\log|\mathbf{I}+\tfrac{1}{\sigma^2}\mathbf{H}\mathbf{Q}_{\text{I}}\mathbf{H}^H|\geq R,\\ & \theta\text{Tr}(\mathbf{Q}_{\text{E}})+(1-\theta)\text{Tr}(\mathbf{Q}_{\text{I}})\leq P,\quad \mathbf{Q}_{\text{E}}\succeq\mathbf{0},\ \mathbf{Q}_{\text{I}}\succeq\mathbf{0},\end{aligned}\tag{25}$$

which is joint convex w.r.t $\mathbf{Q}_{\text{E}}$ and $\mathbf{Q}_{\text{I}}$, and can be solved by using convex optimization methods.

2) Optimal $\theta^\sharp$ for Given $\boldsymbol{Q}_E$ and $\boldsymbol{Q}_I$: With the optimal solution of (25), i.e., $(\mathbf{Q}_{\text{E}}^\sharp, \mathbf{Q}_{\text{I}}^\sharp)$, problem (23) is expressed by

$$\begin{aligned}\max_{\theta}\ & \theta\Psi\left(\text{Tr}(\mathbf{H}\mathbf{Q}_{\text{E}}^\sharp\mathbf{H}^H)\right)\\ \text{s.t. }& (1-\theta)\log|\mathbf{I}+\tfrac{1}{\sigma^2}\mathbf{H}\mathbf{Q}_{\text{I}}^\sharp\mathbf{H}^H|\geq R,\\ & \theta\text{Tr}(\mathbf{Q}_{\text{E}}^\sharp)+(1-\theta)\text{Tr}(\mathbf{Q}_{\text{I}}^\sharp)\leq P,\quad 0\leq\theta\leq 1.\end{aligned}\tag{26}$$

Lemma 5: The optimal solution of problem (26) is

$$\theta^\sharp = \begin{cases}\min\left\{1-\dfrac{R}{\log|\mathbf{I}+\frac{1}{\sigma^2}\mathbf{H}\mathbf{Q}_{\text{I}}^\sharp\mathbf{H}^H|}, \dfrac{P-\text{Tr}(\mathbf{Q}_{\text{I}}^\sharp)}{\text{Tr}(\mathbf{Q}_{\text{E}}^\sharp)-\text{Tr}(\mathbf{Q}_{\text{I}}^\sharp)}\right\}, \\ \qquad\qquad \text{if } \text{Tr}(\mathbf{Q}_{\text{E}}^\sharp)>\text{Tr}(\mathbf{Q}_{\text{I}}^\sharp);\\ 1-\dfrac{R}{\log|\mathbf{I}+\frac{1}{\sigma^2}\mathbf{H}\mathbf{Q}_{\text{I}}^\sharp\mathbf{H}^H|}, \quad \text{if } \text{Tr}(\mathbf{Q}_{\text{E}}^\sharp)\leq\text{Tr}(\mathbf{Q}_{\text{I}}^\sharp).\end{cases}\tag{27}$$

Proof: From the constraint $(1-\theta)\log|\mathbf{I}+\frac{1}{\sigma^2}\mathbf{H}\mathbf{Q}_{\text{I}}^\sharp\mathbf{H}^H|\geq R$, it is known that $\theta\leq 1-\frac{R}{\log|\mathbf{I}+\frac{1}{\sigma^2}\mathbf{H}\mathbf{Q}_{\text{I}}^\sharp\mathbf{H}^H|}$. Moreover, it can be obtained that $\theta(\text{Tr}(\mathbf{Q}_{\text{E}}^\sharp)-\text{Tr}(\mathbf{Q}_{\text{I}}^\sharp))\leq P-\text{Tr}(\mathbf{Q}_{\text{I}}^\sharp)$ from the constraint $\theta\text{Tr}(\mathbf{Q}_{\text{E}}^\sharp)+(1-\theta)\text{Tr}(\mathbf{Q}_{\text{I}}^\sharp)\leq P$. When $\text{Tr}(\mathbf{Q}_{\text{E}}^\sharp)>\text{Tr}(\mathbf{Q}_{\text{I}}^\sharp)$, $\theta\leq\frac{P-\text{Tr}(\mathbf{Q}_{\text{I}}^\sharp)}{\text{Tr}(\mathbf{Q}_{\text{E}}^\sharp)-\text{Tr}(\mathbf{Q}_{\text{I}}^\sharp)}$. When $\text{Tr}(\mathbf{Q}_{\text{E}}^\sharp)<\text{Tr}(\mathbf{Q}_{\text{I}}^\sharp)$, $\theta\geq\frac{P-\text{Tr}(\mathbf{Q}_{\text{I}}^\sharp)}{\text{Tr}(\mathbf{Q}_{\text{E}}^\sharp)-\text{Tr}(\mathbf{Q}_{\text{I}}^\sharp)}$. When $\text{Tr}(\mathbf{Q}_{\text{E}}^\sharp)=\text{Tr}(\mathbf{Q}_{\text{I}}^\sharp)$, θ can be any value within [0, 1]. Besides, the objective function shows that the larger θ, the higher $\theta\Psi\left(\text{Tr}(\mathbf{H}\mathbf{Q}_{\text{E}}^\sharp\mathbf{H}^H)\right)$. According to the above analysis, Lemma 5 is proved. ∎

3) Jointly Optimal θ^*, $\boldsymbol{Q}_E^*$ and $\boldsymbol{Q}_I^*$: Then we find the optimal $(\mathbf{Q}_{\text{E}}^*,\ \mathbf{Q}_{\text{I}}^*,\ \theta^*)$ with an iterative algorithm as described in Algorithm 2, where $\epsilon > 0$ is the termination condition of Algorithm 2.

Algorithm 2 Jointly Optimazing $\mathbf{Q}_{\text{E}}^*$, $\mathbf{Q}_{\text{I}}^*$ and θ^*

1: **Initialization**:
   Set $\theta = \varepsilon$;
   Set $E_{\text{pre}} = 1$ and $E_{\text{cur}} = 0$;
2: **Repeat**:
3: **while** $|E_{\text{cur}} - E_{\text{pre}}| > \epsilon$ **do**
4: Calculate $\mathbf{Q}_{\text{E}}^\sharp$ and $\mathbf{Q}_{\text{I}}^\sharp$ by solving Problem (25);
5: Update $\theta^\sharp$ according to (27);
6: $E_{\text{pre}} = E_{\text{cur}}$;
7: Update $E_{\text{cur}} = \theta^\sharp\Psi\left(\text{Tr}(\mathbf{H}\mathbf{Q}_{\text{E}}^\sharp\mathbf{H}^H)\right)$;
8: **end while**
9: Return $\mathbf{Q}_{\text{E}}^\sharp$, $\mathbf{Q}_{\text{I}}^\sharp$ and $\theta^\sharp$ as the final solution.

Convergence analysis: Let $\mathcal{F} = \theta\Psi\left(\text{Tr}(\mathbf{H}\mathbf{Q}_{\text{E}}\mathbf{H}^H)\right)$. Then, $\frac{\partial\mathcal{F}}{\partial\theta} = \Psi(\text{Tr}(\mathbf{H}\mathbf{Q}_{\text{E}}\mathbf{H}^H)) > 0$ and $\frac{\partial\mathcal{F}}{\partial\mathbf{Q}_{\text{E}}} = \theta\Psi'\left(\text{Tr}(\mathbf{H}\mathbf{Q}_{\text{E}}\mathbf{H}^H)\right)\text{Tr}(\mathbf{H}\mathbf{H}^H) > 0$, which means that $\mathcal{F}$ is an increasing function w.r.t either θ or $\mathbf{Q}_{\text{E}}$. Moreover, according to the constraints in problem (24), it can be inferred that if θ is increased, $\text{Tr}(\mathbf{Q}_{\text{E}})$ decreases, so does $\text{Tr}(\mathbf{H}\mathbf{Q}_{\text{E}}\mathbf{H}^H)$ and $\Psi\left(\text{Tr}(\mathbf{H}\mathbf{Q}_{\text{E}}\mathbf{H}^H)\right)$. When $\theta = 0$, $\mathcal{F} = 0$. If one increases θ from 0 to a small positive number, $\mathcal{F} > 0$, which indicates that $\mathcal{F}$ firstly increases with the increment of θ. Then, if one

goes on increasing θ, whether $\mathcal{F}$ increasing or not will be determined by the contribution of θ and $\mathrm{Tr}(\mathbf{Q}_{\mathrm{E}})$ to $\mathcal{F}$. If the contribution of θ to $\mathcal{F}$ is larger than that of $\mathrm{Tr}(\mathbf{Q}_{\mathrm{E}})$ to $\mathcal{F}$, $\mathcal{F}$ will increase. Otherwise, $\mathcal{F}$ will decrease. It means that $\mathcal{F}$ is an increasing function or a firstly increasing and then decreasing function. For both cases, there exists a maximum $\mathcal{F}^*$. In Algorithm 2, for a given $\mathbf{Q}_{\mathrm{E}}^{\sharp}$ and $\mathbf{Q}_{\mathrm{I}}^{\sharp}$, θ is optimized to increase $\mathcal{F}$, which means that the value of θ associated with current iteration is always larger than that associated with the previous one. If ε is set to be a very small positive number, Algorithm 2 can converge to the optimal $\mathcal{F}^*$.

Proposition 3: The R-E region of the MIMO broadcasting channel with TS receiver under the nonlinear EH model is bounded by that under the linear EH model with $\eta = 1$.

Proof: Similar to the proof of Proposition 2, we have that $E_{\max}^{(\mathrm{nonlinear})} \leq E_{\max}^{(\mathrm{linear})}$ and $R_{\max}^{(\mathrm{nonlinear})} = R_{\max}^{(\mathrm{linear})}$. Moreover, as Problem (24) has the same optimal solution to (25), combining it with Proposition 1, the optimal value of (24) cannot be larger than that of (25), which means that the R-E boundary associated with the nonlinear model from 0 to $R_{\max}$ is bounded by that associated with the linear model with $\eta = 1$. Hence, Proposition 3 is proved. ∎

B. Power Splitting

With power splitting receiver architecture, the received signal at each receiving antenna of the receiver is splitted into two streams by a power splitter with a power splitting factor ρ, where $\sqrt{\rho}$ part is input into the EH receiver and the rest $\sqrt{1-\rho}$ is input into the ID receiver. Similar to [7], we also consider the practical case, where $\sigma_A^2 \ll \sigma_P^2$ and $\sigma^2 = \sigma_A^2 + \sigma_P^2$. σ_A^2 and σ_P^2 are the noise power induced by the antenna and the baseband signal processing, respectively. The R-E region obtained in this case can be approximately regarded as a lower bound of the PS scheme.[3] As the antenna noise can be ignored, it is assumed that $\sigma_A^2 = 0$ and $\sigma_P^2 = 1$. This is equivalent to the situation that the aggregated receiver noise power remains constant with a power splitter at each receiving antenna.

Let ρ_i be the power splitting ratio associated with the i-th receiving antenna, $0 \leq \rho_i \leq 1$ and $i = 1, \ldots, N$. Particularly, when $\rho_i \in \{0, 1\}$, the PS architecture reduces to a new receiver architecture, i.e., antenna switching (AS) architecture, where $\rho_i = 1$ indicates that the i-th antenna is switched to transfer power and $\rho_i = 0$ indicates that the i-th antenna is switched to transmit information. Therefore, AS architecture actually is a special case of PS architecture and PS-based systems have larger R-E regions than AS-based systems. Since our goal is to explore the potential achievable R-E regions of practical MIMO broadcasting channels, we investigate the PS architecture to achieve generality.

[3]With power splitting, the noise of σ_A^2 is divided into two parts, where $(1-\rho)\sigma_A^2$ is input into the information receiver. Thus, the total noise for information decoding is $(1-\rho)\sigma_A^2 + \sigma_P^2$. For a fixed σ^2, since $\sigma_A^2 + \sigma_P^2 = \sigma^2$, when $0 < \sigma_A^2 < \sigma^2$ or $\sigma_A^2 >> \sigma_P^2$, $(1-\rho)\sigma_A^2 + \sigma_P^2 = (1-\rho)\sigma_A^2 + \sigma^2 - \sigma_A^2 = \sigma^2 - \rho\sigma_A^2 < \sigma^2$. But when $\sigma_A^2 \ll \sigma_P^2$, $\sigma_A^2 \to 0$ and $\sigma_P^2 \to \sigma^2$. In this case, $(1-\rho)\sigma_A^2 + \sigma_P^2 \doteq \sigma_P^2 = \sigma^2$, which has the biggest total noise for information decoding and yields the smallest R-E region among all cases [7]. Therefore, when $\sigma_A^2 \ll \sigma_P^2$, the obtained R-E region can be approximately considered as a performance lower bound for the PS scheme with nonlinear EH model.

Define $\mathbf{\Omega}_\rho = \mathrm{diag}(\rho_1, \rho_2, \ldots, \rho_N)$ as the diagonal matrix of the power splitting vector associated with the N receiving antennas, so we have that $\mathbf{0} \preceq_{\mathbb{R}_+^{N_{\mathrm{T}}}} \mathbf{\Omega}_\rho \preceq_{\mathbb{R}_+^{N_{\mathrm{T}}}} \mathbf{I}$. Then, the R-E region of the PS scheme with nonlinear EH model in the worst case can be given by

$$\mathcal{C}_{\text{R-E}}^{(\mathrm{PS})} \triangleq \bigcup_{\mathbf{0} \preceq_{\mathbb{R}_+^{N_{\mathrm{T}}}} \mathbf{\Omega}_\rho \preceq_{\mathbb{R}_+^{N_{\mathrm{T}}}} \mathbf{I}} \Big\{ (R, E) | E \leq \Psi\left(\mathrm{Tr}(\mathbf{\Omega}_\rho \mathbf{H}\mathbf{Q}\mathbf{H}^H)\right), \; R \leq \log|\mathbf{I} + \tfrac{1}{\sigma^2}\bar{\mathbf{\Omega}}_\rho^{\frac{1}{2}}\mathbf{H}\mathbf{Q}\mathbf{H}^H\bar{\mathbf{\Omega}}_\rho^{\frac{1}{2}}|, \; \mathrm{Tr}(\mathbf{Q}) \leq P, \; \mathbf{Q} \succeq \mathbf{0} \Big\}, \tag{28}$$

where $\bar{\mathbf{\Omega}}_\rho = \mathbf{I} - \mathbf{\Omega}_\rho$. $\mathbf{Q}$ is the transmit beamforming covariance matrix, which determines both the transferred energy and information from the transmitter. To figure out the boundary of the R-E region, we consider the following optimization problem,

$$\mathbf{P}_7: \; \max_{\mathbf{Q}, \mathbf{\Omega}_\rho} \; \Psi\left(\mathrm{Tr}(\mathbf{\Omega}_\rho \mathbf{H}\mathbf{Q}\mathbf{H}^H)\right) \quad \text{s.t.} \; \log|\mathbf{I} + \tfrac{1}{\sigma^2}\bar{\mathbf{\Omega}}_\rho^{\frac{1}{2}}\mathbf{H}\mathbf{Q}\mathbf{H}^H\bar{\mathbf{\Omega}}_\rho^{\frac{1}{2}}| \geq R, \quad \mathrm{Tr}(\mathbf{Q}) \leq P, \; \mathbf{Q} \succeq \mathbf{0}, \quad \mathbf{0} \preceq_{\mathbb{R}_+^{N_{\mathrm{T}}}} \mathbf{\Omega}_\rho \preceq_{\mathbb{R}_+^{N_{\mathrm{T}}}} \mathbf{I}. \tag{29}$$

Defining $\mathbf{H}_\rho \triangleq \bar{\mathbf{\Omega}}_\rho^{\frac{1}{2}}\mathbf{H}$ and $\mathbf{F}_\rho \triangleq \mathbf{\Omega}_\rho^{\frac{1}{2}}\mathbf{H}$, (28) can be re-expressed by

$$\max_{\mathbf{Q}, \mathbf{\Omega}_\rho} \Psi\left(\mathrm{Tr}(\mathbf{F}_\rho \mathbf{Q}\mathbf{F}_\rho^H)\right) \quad \text{s.t.} \; \log|\mathbf{I} + \tfrac{1}{\sigma^2}\mathbf{H}_\rho\mathbf{Q}\mathbf{H}_\rho^H| \geq R, \quad \mathrm{Tr}(\mathbf{Q}) \leq P, \; \mathbf{Q} \succeq \mathbf{0}, \quad \mathbf{0} \preceq_{\mathbb{R}_+^{N_{\mathrm{T}}}} \mathbf{\Omega}_\rho \preceq_{\mathbb{R}_+^{N_{\mathrm{T}}}} \mathbf{I}. \tag{30}$$

Since the problem is not joint convex or concave w.r.t. $\mathbf{Q}$ and $\mathbf{\Omega}_\rho$, we analyze and solve it as follows.

1) Optimal $\mathbf{Q}^\sharp$ for Given $\mathbf{\Omega}_\rho$: For a given $\mathbf{\Omega}_\rho$, Problem (30) is reduced to

$$\max_{\mathbf{Q}} \; \Psi\left(\mathrm{Tr}(\mathbf{F}_\rho \mathbf{Q}\mathbf{F}_\rho^H)\right) \quad \text{s.t.} \; \log|\mathbf{I} + \tfrac{1}{\sigma^2}\mathbf{H}_\rho\mathbf{Q}\mathbf{H}_\rho^H| \geq R, \quad \mathrm{Tr}(\mathbf{Q}) \leq P, \; \mathbf{Q} \succeq \mathbf{0}, \tag{31}$$

which has a similar form with Problem $\mathbf{P}_4$ and can be solved by using the same solution method of Problem $\mathbf{P}_4$.

2) Optimal $\mathbf{\Omega}_\rho$ for Given $\mathbf{Q}^\sharp$: With the obtained $\mathbf{Q}^\sharp$, Problem $\mathbf{P}_7$ can be re-expressed as

$$\max_{\mathbf{\Omega}_\rho} \; \Psi\left(\mathrm{Tr}(\mathbf{\Omega}_\rho \mathbf{H}\mathbf{Q}^\sharp\mathbf{H}^H)\right) \quad \text{s.t.} \; \log|\mathbf{I} + \tfrac{1}{\sigma^2}\bar{\mathbf{\Omega}}_\rho^{\frac{1}{2}}\mathbf{H}\mathbf{Q}^\sharp\mathbf{H}^H\bar{\mathbf{\Omega}}_\rho^{\frac{1}{2}}| \geq R, \quad \mathbf{0} \preceq_{\mathbb{R}_+^{N_{\mathrm{T}}}} \mathbf{\Omega}_\rho \preceq_{\mathbb{R}_+^{N_{\mathrm{T}}}} \mathbf{I}, \; \bar{\mathbf{\Omega}}_\rho = \mathbf{I} - \mathbf{\Omega}_\rho, \tag{32}$$

Since $\Psi\left(\mathrm{Tr}(\mathbf{\Omega}_\rho \mathbf{H}\mathbf{Q}^\sharp\mathbf{H}^H)\right)$ is an increasing function of $\mathbf{\Omega}_\rho$ and all constraints in Problem (32) are convex sets, according to Lemma 1 and Lemma 2, Problem (32) has the same optimal solution with the following Problem (33),

$$\max_{\mathbf{\Omega}_\rho} \; \mathrm{Tr}(\mathbf{\Omega}_\rho \mathbf{H}\mathbf{Q}^\sharp\mathbf{H}^H) \quad \text{s.t.} \; \log|\mathbf{I} + \tfrac{1}{\sigma^2}\bar{\mathbf{\Omega}}_\rho^{\frac{1}{2}}\mathbf{H}\mathbf{Q}^\sharp\mathbf{H}^H\bar{\mathbf{\Omega}}_\rho^{\frac{1}{2}}| \geq R, \quad \mathbf{0} \preceq_{\mathbb{R}_+^{N_{\mathrm{T}}}} \mathbf{\Omega}_\rho \preceq_{\mathbb{R}_+^{N_{\mathrm{T}}}} \mathbf{I}, \quad \bar{\mathbf{\Omega}}_\rho = \mathbf{I} - \mathbf{\Omega}_\rho, \tag{33}$$

Lemma 6: By defining $\mathbf{W} \triangleq \boldsymbol{I} + \frac{1}{\sigma^2}\bar{\mathbf{\Omega}}_\rho^{\frac{1}{2}}\boldsymbol{H}\boldsymbol{Q}^\sharp\boldsymbol{H}^H\bar{\mathbf{\Omega}}_\rho^{\frac{1}{2}}$, *Problem (33) can be equivalently transformed into the following problem*

$$\begin{aligned}&\min_{\mathbf{W}}\ \sigma^2\mathrm{Tr}(\mathbf{W}) - \mathrm{Tr}(\mathbf{H}\mathbf{Q}^\sharp\mathbf{H}^H) - \sigma^2\mathrm{Tr}(\mathbf{I})\\ &\text{s.t. } \log|\mathbf{W}| \geq R, \quad \mathbf{I}\preceq_{\mathbb{R}_+^{N_\mathrm{T}}}\mathbf{W}\preceq_{\mathbb{R}_+^{N_\mathrm{T}}}\mathbf{I}+\mathbf{H}\mathbf{Q}^\sharp\mathbf{H}^H,\ \mathbf{W}\succeq\mathbf{0}.\end{aligned} \tag{34}$$

Proof: The proof of Lemma 6 can be found in Appendix C. ∎

Problem (34) is a convex optimization problem and can be solved by using some solution methods for convex optimization problems, such as interior point method [36]. Once the optimal $\mathbf{W}^\sharp$ is obtained, we can calculate $\mathbf{\Omega}_\rho$ as follows. Let w_i be the i-th diagonal entry of matrix $\mathbf{W}^\sharp - \mathbf{I}$ and d_i be the i-th diagonal entry of matrix $\mathbf{H}\mathbf{Q}^\sharp\mathbf{H}^H$, where $i = 1, 2, \ldots, N$. According to $\mathbf{W} \triangleq \mathbf{I} + \frac{1}{\sigma^2}\bar{\mathbf{\Omega}}_\rho^{\frac{1}{2}}\mathbf{H}\mathbf{Q}^\sharp\mathbf{H}^H\bar{\mathbf{\Omega}}_\rho^{\frac{1}{2}}$, the entries of $\mathbf{W}$ are equal to the corresponding entries of $\mathbf{I} + (\mathbf{I} - \mathbf{\Omega}_\rho)^{\frac{1}{2}}\mathbf{H}\mathbf{Q}^\sharp\mathbf{H}^H(\mathbf{I} - \mathbf{\Omega}_\rho)^{\frac{1}{2}}$, which indicates that $w_i = (1 - \rho_i) * d_i$. Therefore, $\mathbf{\Omega}_\rho^\sharp$ can be given by

$$\mathbf{\Omega}_\rho^\sharp = \mathrm{diag}(1 - \tfrac{w_1}{d_1}, 1 - \tfrac{w_2}{d_2}, \ldots, 1 - \tfrac{w_N}{d_N}). \tag{35}$$

3) Jointly Optimal $\boldsymbol{Q}^*$ and $\mathbf{\Omega}_\rho^*$: Based on above calculations, the jointly optimizing $\mathbf{Q}^*$ and $\mathbf{\Omega}_\rho^*$ can be obtained by using Algorithm 3, where $\epsilon > 0$ is the termination condition of Algorithm 3.

Algorithm 3 Jointly Optimizing $\mathbf{Q}^*$ and $\mathbf{\Omega}_\rho^*$

1: **Initialization**:
   Set $\mathbf{\Omega}_\rho = [\varepsilon\ \varepsilon\ \ldots\ \varepsilon]$;
   Set $E_{\mathrm{pre}} = 1$ and $E_{\mathrm{cur}} = 0$;
2: **Repeat**:
3: **while** $|E_{\mathrm{cur}} - E_{\mathrm{pre}}| > \epsilon$ **do**
4: Calculate $\mathbf{Q}^\sharp$ by solving Problem (31);
5: Calculate $\mathbf{W}^\sharp$ by solving Problem (34);
6: Update $\mathbf{\Omega}_\rho$ according to (35);
7: $E_{\mathrm{pre}} = E_{\mathrm{cur}}$;
8: Update $E_{\mathrm{cur}} = \Psi\left(\mathrm{Tr}(\mathbf{\Omega}_\rho^\sharp\mathbf{H}\mathbf{Q}^\sharp\mathbf{H}^H)\right)$;
9: **end while**
10: Return $\mathbf{Q}^\sharp$ and $\mathbf{\Omega}_\rho^\sharp$ as the final optimal solution.

Convergence analysis: It is known that $\mathrm{Tr}(\mathbf{Q})$ represents the transmit power and $\mathrm{Tr}(\mathbf{\Omega}_\rho\mathbf{H}\mathbf{Q}\mathbf{H}^H)$ represents the received RF power. Higher transmit power leads to higher received RF power, so $\mathrm{Tr}(\mathbf{\Omega}_\rho\mathbf{H}\mathbf{Q}\mathbf{H}^H)$ increases with the increment of $\mathrm{Tr}(\mathbf{Q})$. For a given $\mathbf{\Omega}_\rho$, to maximize $\mathrm{Tr}(\mathbf{\Omega}_\rho\mathbf{H}\mathbf{Q}\mathbf{H}^H)$, $\mathrm{Tr}(\mathbf{Q})$ should be its maximum value P. In this case, if $\log|\mathbf{I} + \frac{1}{\sigma^2}\mathbf{H}_\rho\mathbf{Q}\mathbf{H}_\rho^H| > R$, $\mathbf{\Omega}_\rho$ can be increased to improve $\mathrm{Tr}(\mathbf{\Omega}_\rho\mathbf{H}\mathbf{Q}\mathbf{H}^H)$. Until when $\log|\mathbf{I} + \frac{1}{\sigma^2}\mathbf{H}_\rho\mathbf{Q}\mathbf{H}_\rho^H| = R$, $\mathbf{\Omega}_\rho$ cannot be increased any more, so does $\mathrm{Tr}(\mathbf{\Omega}_\rho\mathbf{H}\mathbf{Q}\mathbf{H}^H)$. Therefore, there exists a maximum $\mathrm{Tr}(\mathbf{\Omega}_\rho\mathbf{H}\mathbf{Q}\mathbf{H}^H)$. In Algorithm 3, for a given $\mathbf{Q}^\sharp$, $\mathbf{\Omega}_\rho$ is optimized to increase $\mathrm{Tr}(\mathbf{\Omega}_\rho\mathbf{H}\mathbf{Q}\mathbf{H}^H)$, which means that $\mathbf{\Omega}_\rho$ associated with current iteration is always increased over the proper cone $\mathbb{R}_+^{N_\mathrm{T}}$ compared with that associated with the previous iteration. Therefore, with a small positive value of ε, Algorithm 3 can converge to the optimal $\Psi\left(\mathrm{Tr}(\mathbf{\Omega}_\rho\mathbf{H}\mathbf{Q}^\sharp\mathbf{H}^H)\right)$.

Proposition 4: The R-E region of the MIMO broadcasting channel with PS receiver architecture under the nonlinear EH model is bounded by that under linear EH model with $\eta = 1$.

Proof: Similar to the proof of Proposition 2, we have that $E_{\max}^{(\mathrm{nonlinear})} \leq E_{\max}^{(\mathrm{linear})}$ and $R_{\max}^{(\mathrm{nonlinear})} = R_{\max}^{(\mathrm{linear})}$. Moreover, since Problem (32) has the same optimal solution with Problem (33), combining it with Proposition 1, the optimal value of Problem (32) cannot be larger than that of Problem (33). Besides, from the solution method for Problem (31), it is also known that the optimal value of Problem (31) must be equal or smaller than that associated with the linear EH model. As a result, the optimal value of Problem $\mathbf{P}_7$ also must be equal or smaller that the optimization problem associated with the linear EH model, which means that the boundary curve associated with the nonlinear model from 0 to $R_{\max}$ is bounded by that associated with the linear model with $\eta = 1$. Therefore, Proposition 4 is proved. ∎

V. Numerical Results and Discussion

This section provides some numerical results to show the R-E region of the SWIPT MIMO broacasting channel with nonlinear EH model. In the simulations, the system bandwidth is set to be 1MHz. The receiver antenna noise power density is -100dBm/Hz. Path loss factor is assumed to be 4 and the available transmit power at the transmitter is 2Watt. For comparison, the R-E region of the SWIPT MIMO broacasting channel with traditional linear EH model is also simulated, where η is set to 1 and the R-E region of the linear EH model system is derived by solving the corresponding optimization problem in [7]. For our considered nonlinear EH model, two groups of circuit parameters, i.e., $(a = 6400, b = 0.003)$ and $(a = 1500, b = 0.0022)$ provided by [28], [37], [38], and [39], are adopted, and the R-E region of the nonlinear EH model system is calculated with our newly obtained theoretical results and the algorithms in this paper. In order to clearly show the difference performance of linear EH model and the nonlinear EH model, we illustrate the linear EH model and the nonlinear EH model as shown in Figure 2, where the harvested energy versus the input RF power is plotted. For the linear EH model, it is with $\eta = 1$ and for the nonlinear EH model, it is generated in terms of (2) with the parameters mentioned previously. These system configurations and parameter settings will not change unless otherwise specified.

Note that M indicates the maximum harvested power at receiver when the EH circuit is saturated. In practical systems, the values of M are determined by EH circuits and may be much different due to circuit designs. In the simulations, we just want to show the effect trends of different values of M on system R-E regions rather than real values of M. As described in Proposition 1, the maximum harvested energy of nonlinear EH model is also bounded by that of the linear EH model, i.e., $E_{\max}$. Thus, when $M > E_{\max}$, the maximum harvested energy of nonlinear EH model is not larger than $E_{\max}$. Therefore, we select $E_{\max}$ as a reference value of

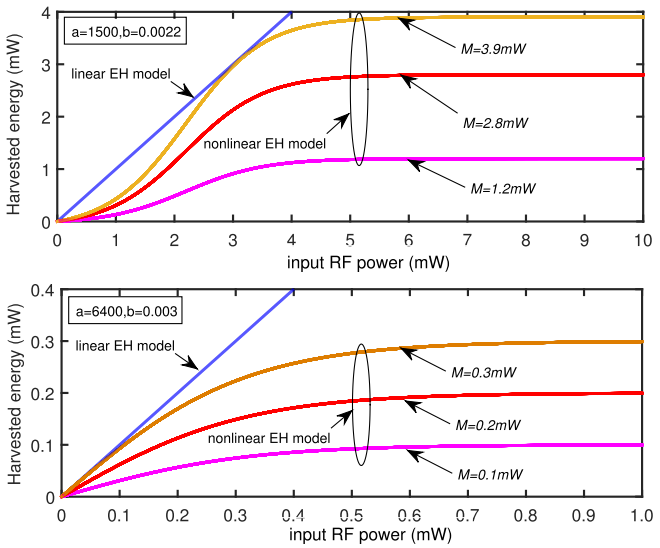

Fig. 2. Illustration of the linear EH model and the nonlinear EH model with different circuit parameters, where two groups of circuit parameters, i.e., $(a = 6400, b = 0.003)$ and $(a = 1500, b = 0.0022)$ provided by [28], [37], [38], and [39], are adopted.

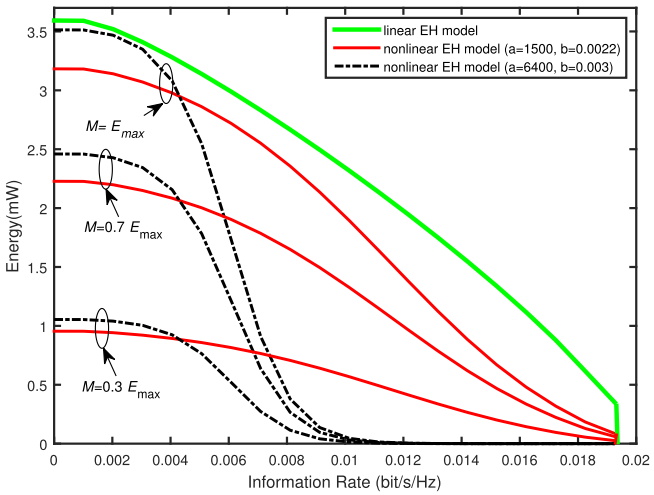

Fig. 3. Example 1: R-E region of MIMO broadcasting channel with separated receivers for specified $\mathbf{H}_{\mathrm{E}}$ and $\mathbf{H}_{\mathrm{I}}$, where $N_{\mathrm{T}} = N_{\mathrm{E}} = N_{\mathrm{I}} = 2$.

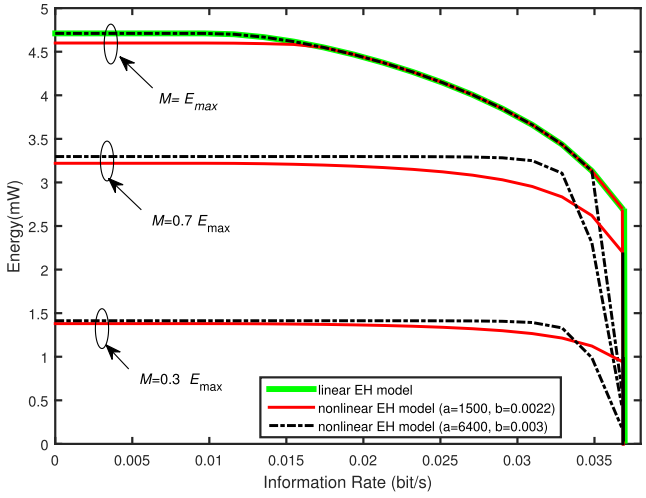

Fig. 4. Example 2: R-E region of MIMO broadcasting channel with separated receivers for specified $\mathbf{H}_{\mathrm{E}}$ and $\mathbf{H}_{\mathrm{I}}$, where $N_{\mathrm{T}} = N_{\mathrm{E}} = N_{\mathrm{I}} = 4$.

maximum M, and select $0.7E_{\max}$ and $0.3E_{\max}$ to show the effect trends of different M on system performance.

A. R-E Region of the Separated Receivers Scenario

Firstly, we provide some results to show the R-E region of MIMO broadcasting channel with separated EH and ID receivers. In the simulations, the distances between the transmitter and the EH receiver and between the transmitter and the ID receiver were set to be 7m and 50m, respectively. The channels were generated following Rayleigh distribution.

In Figure 3 and Figure 4, we provide two examples with specified channel matrices to show the R-E region of the MIMO channel with separated EH and ID receivers, where $N_{\mathrm{T}} = N_{\mathrm{E}} = N_{\mathrm{I}} = 2$ in Figure 3 and $N_{\mathrm{T}} = N_{\mathrm{E}} = N_{\mathrm{I}} = 4$ in Figure 4. In Figure 3, $\mathbf{H}_{\mathrm{E}} = [-0.0583 + 0.5942i \; -0.3104 + 0.0708i; \; -1.3669 - 0.6279i \; -1.2690 - 0.3850i]$ and $\mathbf{H}_{\mathrm{I}} = [0.2146 + 1.2105i \; 0.3465 - 1.5120i; \; -0.4245 - 0.1373i \; 0.5228 - 0.5937i]$ and in Figure 4, $\mathbf{H}_{\mathrm{E}}$ and $\mathbf{H}_{\mathrm{I}}$ are respectively shown in (36) and (37), as shown at the bottom of this page. In both figures, $M = E_{\max}$, $M = 0.7E_{\max}$ and $M = 0.3E_{\max}$ are considered, where $E_{\max}$ is obtained in terms of $E_{\max} = h_1^{(\mathrm{e})} P$, which is the maximum energy that can be harvested over the MIMO channel with the linear EH model. It can be observed that for the same (a, b)-pair configuration, the larger the value of M, the larger the R-E region. The reason is that a larger M may bring a higher maximum power (when the EH circuit is saturated) that can be harvested at the EH receiver. Moreover, for the same M, the R-E regions associated with different pairs of (a, b) show very different boundary shapes. Specifically, with the increment of R, the maximal harvested energy of the system with $(a = 6400, b = 0.003)$

$$\mathbf{H}_{\mathrm{E}} = \begin{bmatrix} 0.1907 - 0.2069i & -0.3161 - 0.3486i & 0.8921 + 0.4323i & -0.4644 + 1.2760i \\ 0.3495 - 0.3824i & 0.0775 - 0.1278i & 0.3362 + 0.0773i & -1.0475 - 0.5113i \\ -1.0487 - 0.2182i & 0.7981 + 0.0324i & 0.8302 + 1.2827i & 0.1099 + 0.3723i \\ -0.7214 - 0.7754i & -0.2050 - 0.0451i & 0.0898 + 0.2206i & 0.5788 - 0.1840i \end{bmatrix} \tag{36}$$

$$\mathbf{H}_{\mathrm{I}} = \begin{bmatrix} 0.4244 - 0.3006i & -1.0190 - 0.6945i & 0.5744 - 0.4429i & -0.5317 - 0.4531i \\ 0.4200 + 0.4168i & 0.2841 + 0.4331i & 0.3858 + 0.1764i & 1.0722 + 1.2791i \\ -1.5458 - 0.0444i & 1.0396 - 0.0388i & -0.7436 - 0.7022i & -0.0230 - 0.7636i \\ -0.9384 - 1.4297i & -0.2311 - 0.7911i & 0.2811 + 0.6894i & 1.1568 + 0.1408i \end{bmatrix} \tag{37}$$

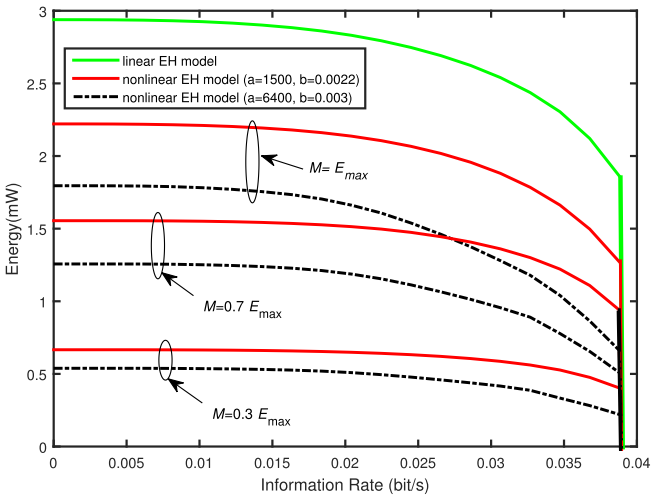

Fig. 5. Average R-E region of MIMO broadcasting channel with separated receivers, where $N_{\mathrm{T}} = N_{\mathrm{E}} = N_{\mathrm{I}} = 2$.

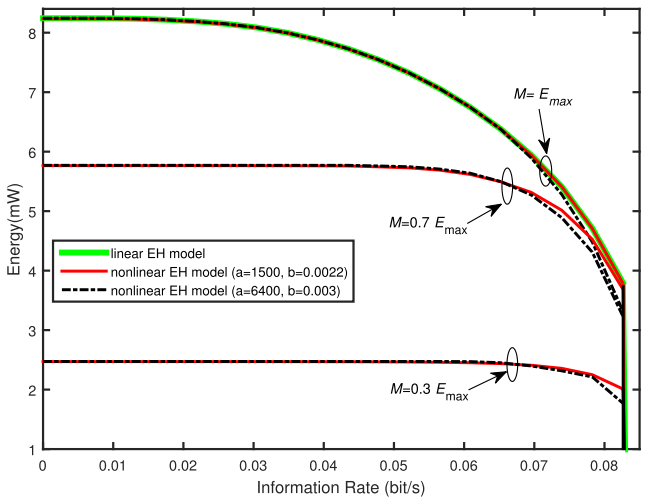

Fig. 6. Average R-E region of MIMO broadcasting channel with separated receivers, where $N_{\mathrm{T}} = N_{\mathrm{E}} = N_{\mathrm{I}} = 4$.

declines much faster than that of the system with $(a = 1500, b = 0.0022)$, but the maximal harvested energy of the system with $(a = 6400, b = 0.003)$ decreases later than that of the system with $(a = 1500, b = 0.0022)$. Besides, the declining rate of the system with $(a = 6400, b = 0.003)$ first increases and then decreases while that of the system with $(a = 6400, b = 0.003)$ gradually increases. The reason is that different values of (a, b) yield very different EH behaviors, as shown in Figure 2 of [28]. For the EH circuit with $(a = 6400, b = 0.003)$, the increasing rate of the harvested power decreases with the increment of the input RF power, but for the EH circuit with $(a = 1500, b = 0.0022)$, the increasing rate of the harvested power first increases and then decreases with the increment of the input RF power. Additionally, it is also observed that the R-E regions associated with the nonlinear EH model are covered by the regions associated with the linear EH model,[4] which is consistent with Proposition 2. Particularly, in Figure 4, a part of the boundary of the R-E region associated with $M = E_{\max}, a = 1500, b = 0.0022$ overlaps that of the traditional linear EH model, which implies that with some proper circuit parameters and certain channel gains, the R-E region obtained with the traditional linear EH model may be achievable in practical non-linear systems.

In Figure 5 and Figure 6, the average R-E regions of the MIMO broadcasting channel with separated EH and ID receivers are plotted for $N_{\mathrm{T}} = N_{\mathrm{E}} = N_{\mathrm{I}} = 2$ and $N_{\mathrm{T}} = N_{\mathrm{E}} = N_{\mathrm{I}} = 4$, respectively. Every point on the boundary of the R-E region was averaged over 100 channel realizations. From the two figures, the average R-E region associated with $(a = 6400, b = 0.003)$ is always a subset of the corresponding one associated with $(a = 1500, b = 0.0022)$, which means the circuit with parameters $(a = 1500, b = 0.0022)$ has better average system performance than that of the circuit with parameters $(a = 6400, b = 0.003)$. Moreover, the average

[4]This does not means that the linear EH model is superior to the nonlinear EH model, as the the R-E region obtained with the EH model actually may not always be achievable in practical systems due to the nonlinear EH circuit features.

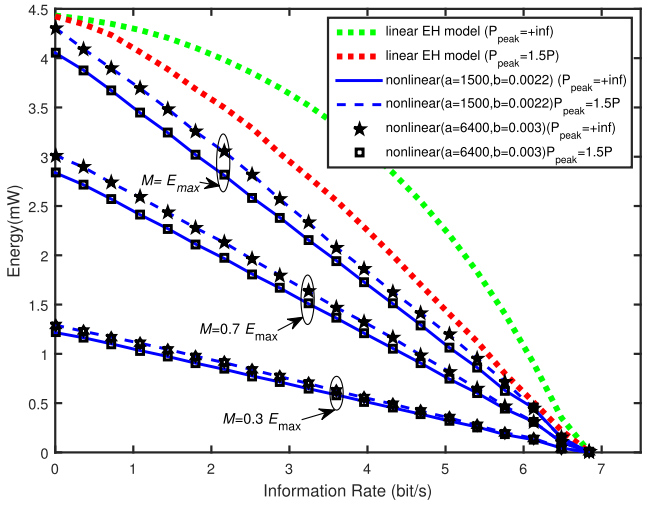

Fig. 7. An example of the R-E region of MIMO broadcasting channel for a specified $\mathbf{H}$ with TS receiver architecture.

R-E region associated with the $4 \times 4 \times 4$-antenna system is larger than that associated with the $2 \times 2 \times 2$-antenna system, which means that by equipping more antennas in SWIPT systems, a larger R-E region can be achieved.

B. R-E Region of Co-Located Receivers Scenario

Secondly, we provide some results to show the R-E region of MIMO broadcasting channel with co-located EH and ID receivers. In the simulations, the distances between the transmitter and the receiver was set to be 8m. The channels were also generated following Rayleigh distribution.

In Figure 7, we present an example of the R-E region of a 2×2 MIMO broadcasting channel with TS receiver architecture, where $\mathbf{H} = [-0.1241 + 0.6715i \ 1.4090 + 0.7172i; \ 1.4897 - 1.2075i \ 1.4172 + 1.6302i]$. In (22), P_{peak} is not confined, which means that P_{peak} in (22) is allowed to be $+\mathrm{inf}$. In this case, the obtained R-E region can be considered as an outer bound but it may not always

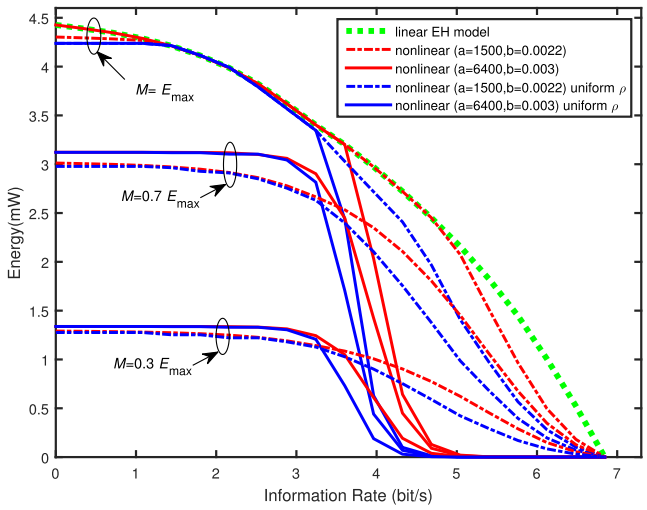

Fig. 8. An example of the R-E region of MIMO broadcasting channel for a specified **H** with PS receiver architecture.

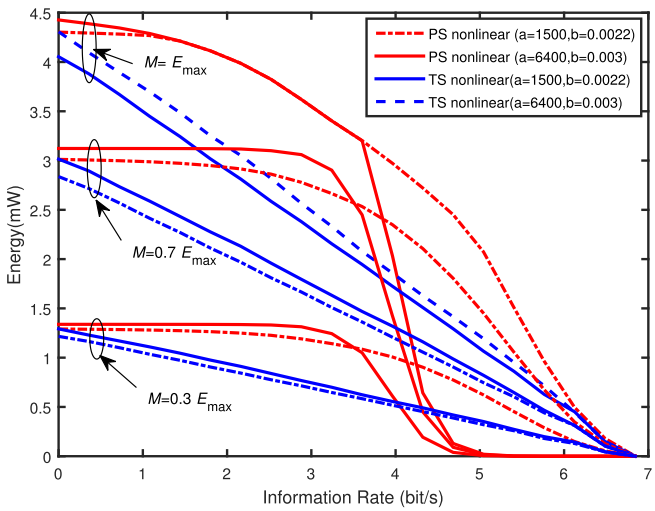

Fig. 9. Comparison of R-E region of MIMO broadcasting channel with a specified **H** for TS and PS receivers.

be practical. Thus, we also simulate the R-E region of the TS system with the peak power constraint, i.e., $P_{\text{peak}} \leq 1.5P$. In Figure 7, for the same M, the systems with different pairs of (a, b) have different R-E regions. The system with $(a = 6400, b = 0.003)$ has a larger R-E region than that with $(a = 1500, b = 0.0022)$. Moreover, the smaller M results in a smaller R-E region, which means that in the co-located receivers system with TS receiver architecture, both M and (a, b) affect the system R-E tradeoff greatly. Besides, the R-E region of the system with nonlinear EH model under the peak power constraint of $P_{\text{peak}} \leq 1.5P$ is very close to that under $P_{\text{peak}} \leq +inf$. It is also observed that the R-E region of the TS system under nonlinear EH model is bounded within that of the TS system under traditional linear EH model, which is consistent with Proposition 3. With the same channel and system configuration, Figure 8 plot the R-E region of the 2×2 MIMO broadcasting channel with PS receiver architecture. The system with uniformed ρ where $\rho_1 = \rho_2 = \cdots = \rho_N$ was also simulated for comparison. As expected, the system with uniformed ρ achieves smaller R-E region compared with the system with flexible ρ, but the R-E region shape does not change obviously. Moreover, the maximum harvested energy associated with the system with uniformed ρ is obviously lower than that of the system with flexible ρ at the relatively high R regime. It is also observed that the R-E region of the PS system under nonlinear EH model is bounded within that of the PS system under traditional linear EH model, which is consistent with Proposition 4.

Figure 9 compares the R-E regions of the 2×2 MIMO broadcasting channel with PS and TS receiver architectures under the nonlinear EH model, where the channel matrix **H** is the same with that of Figure 7. It is observed that for the same system parameters, the TS system shows very different R-E tradeoff behaviour from PS system. That is, with the increment of R, the maximum harvested energy gradually decreases in the TS system while the maximum harvested energy keeps stable at first and then sharply decreases in the PS system. For a relatively small R, the maximum harvested energy of the PS system is higher than that of the TS system, but for a relatively large R, the maximum harvested energy of the PS system is lower than that of the TS system.

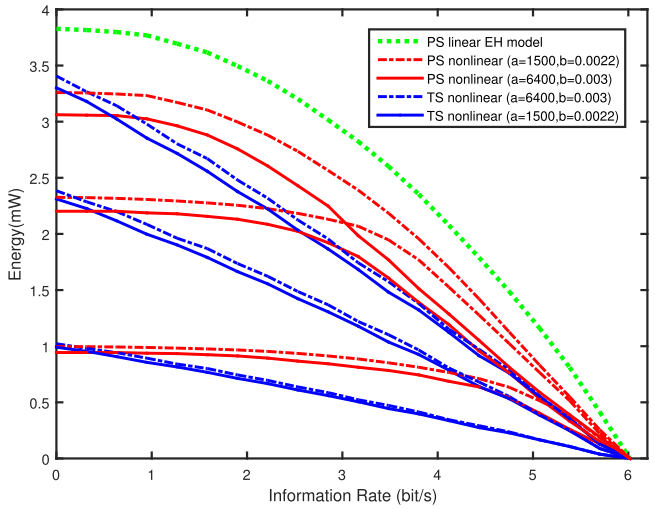

Fig. 10. Average R-E region of MIMO broadcasting channel with co-located TS and PS receivers, where $N = 2$.

In Figure 10, the average R-E regions of the MIMO broadcasting channel with colocated EH and ID receivers are plotted for $N_{\text{T}} = N_{\text{E}} = N_{\text{I}} = 2$. Both TS and PS receiver architectures are simulated. Each point on the boundary of the R-E region is obtained by averaging 100 randomly generated channel realizations. It can be observed that the PS system has very different system performance compared with the TS system. For the same M, the PS system with $(a = 1500, b = 0.0022)$ achieves larger R-E region than that with $(a = 6400, b = 0.003)$, but the TS system with $(a = 1500, b = 0.0022)$ achieves smaller R-E region than that with $(a = 6400, b = 0.003)$. Moreover, for the PS system, with the increment of R the maximum harvested energy first decrease very slowly and then decreases more and more sharply, while for the TS system, with the increment of R the maximum harvested

energy decreases almost with the same rate. Besides, with the same system parameter configuration, the R-E region of the PS system is almost always larger than that of the TS system, which means PS system is able to achieve better average R-E tradeoff for MIMO broadcasting channel.

From the simulation results in this section, we obtain the following results. 1) The variation of M greatly affects the size of the R-E region of the MIMO broadcasting channel with nonlinear EH model. 2) The parameters a and b determine the shape of R-E region of the MIMO broadcasting channel with nonlinear EH model. 3) The R-E region of the nonlinear EH model system is bounded by that of linear EH model system with $\eta = 1$. Nevertheless, the R-E region yielded by the nonlinear EH model is more reasonable, which is much closer to practice than that yielded by the linear EH ymodel. 4) Basically, with the same system parameters, the PS system always outperforms TS system under the nonlinear EH ymodel.

VI. Conclusion

This paper studied the R-E region for MIMO broadcasting channel under the nonlinear EH ymodel. Two different scenarios were considered, i.e., the separated EH and ID receivers scenario and the co-located EH yand ID receivers scenario. For the latter scenario, two practical receiver architectures, i.e., TS and PS receiver architectures were investigated. By considering such a typical MIMO broadcasting system, several optimization problems were formulated to derive the boundary of the R-E region for the considered systems. As the problems were non-convex, we derived some semi-closed-form solutions and then designed efficient algorithms to solve them. Numerical results were provided to show the R-E regions of the systems, which provide some interesting insights. It is shown that all practical circuit specifications greatly affect the system R-E region. Compared with the systems under current linear EH model, the ones under the practical nonlinear EH model achieve smaller R-E regions and show different R-E tradeoff behaviors. With the increment of R, the average maximum harvested energy in the separated EH and ID receivers system and in the PS system decreases with an increasing declining rate, but decreases with an almost constant declining rate in the PS system. Besides, the PS system achieves larger average R-E region than the TS one. These results may provide some useful insights for better understanding the multi-antenna SWIPT system with nonlinear EH model. In this work, only one ID and EH receivers were considered. In our future work, we shall investigate the system with more ID and EH receivers.

Appendix A
The Proof of Lemma 4

For a given μ and ν, (16) can be equivalently re-expressed by

$$\max_{\mathbf{Q}\succeq 0}\ \mathrm{Tr}\left((\mathbf{H}_{\mathrm{E}}^H\mathbf{H}_{\mathrm{E}}-\nu\mathbf{I})\mathbf{Q}\right)+\mu\log|\,\mathbf{I}+\tfrac{1}{\sigma_{\mathrm{I}}^2}\mathbf{H}_{\mathrm{I}}\mathbf{Q}\mathbf{H}_{\mathrm{I}}^H\,| \quad (38)$$

Let $\mathbf{Q}=\zeta\boldsymbol{v}_{\mathrm{E}}^{(1)}(\boldsymbol{v}_{\mathrm{E}}^{(1)})^H$, where ζ is a positive constant. Substituting $\mathbf{Q}=\zeta\boldsymbol{v}_{\mathrm{E}}^{(1)}(\boldsymbol{v}_{\mathrm{E}}^{(1)})^H$ into the objective function of (38), we have that

$$\begin{aligned}
&\mathrm{Tr}\left((\mathbf{H}_{\mathrm{E}}^H\mathbf{H}_{\mathrm{E}}-\nu\mathbf{I})\mathbf{Q}\right)+\mu\log|\,\mathbf{I}+\tfrac{1}{\sigma_{\mathrm{I}}^2}\mathbf{H}_{\mathrm{I}}\mathbf{Q}\mathbf{H}_{\mathrm{I}}^H\,|\\
&=\mathrm{Tr}((\mathbf{H}_{\mathrm{E}}^H\mathbf{H}_{\mathrm{E}}\zeta\boldsymbol{v}_{\mathrm{E}}^{(1)}(\boldsymbol{v}_{\mathrm{E}}^{(1)})^H)-\mathrm{Tr}(\nu\mathbf{I}\zeta\boldsymbol{v}_{\mathrm{E}}^{(1)}(\boldsymbol{v}_{\mathrm{E}}^{(1)})^H)\\
&\quad+\mu\log|\,\mathbf{I}+\tfrac{1}{\sigma_{\mathrm{I}}^2}\parallel\mathbf{H}_{\mathrm{I}}\boldsymbol{v}_{\mathrm{E}}^{(1)}\parallel^2|\\
&=\zeta\mathrm{Tr}((\boldsymbol{v}_{\mathrm{E}}^{(1)})^H\mathbf{H}_{\mathrm{E}}^H\mathbf{H}_{\mathrm{E}}\boldsymbol{v}_{\mathrm{E}}^{(1)})-\nu\zeta\mathrm{Tr}((\boldsymbol{v}_{\mathrm{E}}^{(1)})^H\mathbf{I}\boldsymbol{v}_{\mathrm{E}}^{(1)})\\
&\quad+\mu\log|\,\mathbf{I}+\tfrac{\zeta}{\sigma_{\mathrm{I}}^2}\parallel\mathbf{H}_{\mathrm{I}}\boldsymbol{v}_{\mathrm{E}}^{(1)}\parallel^2|\\
&=\zeta\lambda_1-\nu\zeta+\mu\log|\,\mathbf{I}+\tfrac{\zeta}{\sigma_{\mathrm{I}}^2}\parallel\mathbf{H}_{\mathrm{I}}\boldsymbol{v}_{\mathrm{E}}^{(1)}\parallel^2|=\zeta(\lambda_1-\nu)\\
&\quad+\mu\log|\,\mathbf{I}+\tfrac{\zeta}{\sigma_{\mathrm{I}}^2}\parallel\mathbf{H}_{\mathrm{I}}\boldsymbol{v}_{\mathrm{E}}^{(1)}\parallel^2|\,. \qquad (39)
\end{aligned}$$

For given μ and ν, it can be seen that if $\nu\le\lambda_1$, when $\zeta\to\infty$, $\zeta(\lambda_1-\nu)+\mu\log|\,\mathbf{I}+\frac{\zeta}{\sigma_{\mathrm{I}}^2}\parallel\mathbf{H}_{\mathrm{I}}\boldsymbol{v}_{\mathrm{E}}^{(1)}\parallel^2|$ will be unbounded. That is, if $\nu<\lambda_1$, the optimal value of Problem (38) will be infinity, which is a non-reasonable result. Therefore, it must be satisfied that $\nu>\lambda_1$.

Appendix B
The Proof of Theorem 1

Define $\mathbf{B}\triangleq\nu\mathbf{I}-\mathbf{H}_{\mathrm{E}}^H\mathbf{H}_{\mathrm{E}}$. It follows that when $\nu>\lambda_1$, $\mathbf{B}\succeq\mathbf{0}$ and $\mathbf{B}^{-1}$ exists. Then Problem (38) can be re-written to be

$$\begin{aligned}
&\max_{\mathbf{Q}\succeq 0}\ \mu\log|\,\mathbf{I}+\tfrac{1}{\sigma_{\mathrm{I}}^2}\mathbf{H}_{\mathrm{I}}\mathbf{Q}\mathbf{H}_{\mathrm{I}}^H\,|-\mathrm{Tr}\,(\mathbf{B}\mathbf{Q})\\
&\quad\equiv\max_{\mathbf{Q}\succeq 0}\ \mu\log|\,\mathbf{I}+\tfrac{1}{\sigma_{\mathrm{I}}^2}\mathbf{H}_{\mathrm{I}}\mathbf{Q}\mathbf{H}_{\mathrm{I}}^H\,|-\mathrm{Tr}\left(\mathbf{B}^{\frac{1}{2}}\mathbf{B}^{\frac{1}{2}}\mathbf{Q}\right) \qquad (40)
\end{aligned}$$

Let $\mathbf{F}=\mathbf{B}^{\frac{1}{2}}\mathbf{Q}\mathbf{B}^{\frac{1}{2}}$. So, $\mathbf{Q}=\mathbf{B}^{-\frac{1}{2}}\mathbf{F}\mathbf{B}^{-\frac{1}{2}}$. Then (40) is further expressed by

$$\max\nolimits_{\mathbf{F}\succeq 0}\ \mu\log|\,\mathbf{I}+\tfrac{1}{\sigma^2}\mathbf{H}_{\mathrm{I}}\mathbf{B}^{-\frac{1}{2}}\mathbf{F}\mathbf{B}^{-\frac{1}{2}}\mathbf{H}_{\mathrm{I}}^H\,|-\mathrm{Tr}\,(\mathbf{F}) \qquad (41)$$

Let $f(\mathbf{F})=\mu\log|\,\mathbf{I}+\frac{1}{\sigma^2}\mathbf{H}_{\mathrm{I}}\mathbf{B}^{-\frac{1}{2}}\mathbf{F}\mathbf{B}^{-\frac{1}{2}}\mathbf{H}_{\mathrm{I}}^H\,|-\mathrm{Tr}\,(\mathbf{F})$. It can be seen that $f(\mathbf{F})$ is a concave function w.r.t. $\mathbf{F}$, so its maximum value is achieved at the stationary point, i.e., $\frac{\partial f(\mathbf{F})}{\partial\mathbf{F}}\Big|_{\mathbf{F}=\mathbf{F}^*}=0$. Thus, $\mathbf{F}^*$ can be obtained by letting $\frac{\partial f(\mathbf{F})}{\partial\mathbf{F}}=0$.

Let $\mathbf{Z}$ be a matrix satisfying that $\frac{1}{\sigma_{\mathrm{I}}^2}\mathbf{H}_{\mathrm{I}}\mathbf{B}^{-\frac{1}{2}}\mathbf{Z}\mathbf{B}^{-\frac{1}{2}}\mathbf{H}_{\mathrm{I}}^H=\mathbf{I}$. It can be obtained that

$$\begin{aligned}
f(\mathbf{F})&=\mu\log|\tfrac{1}{\sigma_{\mathrm{I}}^2}\mathbf{H}_{\mathrm{I}}\mathbf{B}^{-\frac{1}{2}}(\mathbf{Z}+\mathbf{F})\mathbf{B}^{-\frac{1}{2}}\mathbf{H}_{\mathrm{I}}^H|-\mathrm{Tr}\,(\mathbf{F})\\
&=\tfrac{\mu}{\sigma_{\mathrm{I}}^{2N_{\mathrm{I}}}}\left(\log|\mathbf{H}_{\mathrm{I}}\mathbf{B}^{-\frac{1}{2}}|+\log|(\mathbf{Z}+\mathbf{F})|+\log|\mathbf{B}^{-\frac{1}{2}}\mathbf{H}_{\mathrm{I}}^H|\right)\\
&\quad-\mathrm{Tr}\,(\mathbf{F})\,.
\end{aligned}$$

With $\frac{\partial f(\mathbf{F})}{\partial\mathbf{F}}=\frac{\mu}{\sigma_{\mathrm{I}}^{2N_{\mathrm{I}}}}\frac{1}{(\mathbf{F}+\mathbf{Z})\ln 2}-\mathbf{I}=0$, we get that

$$\mathbf{F}^*=\tfrac{\mu}{\sigma_{\mathrm{I}}^{2N_{\mathrm{I}}}\ln 2}\mathbf{I}-\mathbf{Z}. \qquad (42)$$

By performing SVD on matrix $\mathbf{H}_{\mathrm{I}}\mathbf{B}^{-\frac{1}{2}}$, we have $\mathbf{H}_{\mathrm{I}}\mathbf{B}^{-\frac{1}{2}}=\hat{\mathbf{U}}\boldsymbol{\Lambda}_{\mathrm{H_IB}}\hat{\mathbf{V}}^H$, where $\boldsymbol{\Lambda}_{\mathrm{H_IB}}=\mathrm{diag}(\sqrt{\lambda_1},\sqrt{\lambda_2},\ldots.\sqrt{\lambda_{\min\{N_{\mathrm{T}},N_{\mathrm{I}}\}}})$ with $\lambda_1\ge\lambda_2\ge\ldots\ge\lambda_{\min\{N_{\mathrm{T}},N_{\mathrm{I}}\}}\ge 0$. Thus, $\mathbf{Z}=\hat{\mathbf{V}}(\boldsymbol{\Lambda}_{\mathrm{H_IB}})^{-1}\hat{\mathbf{U}}^H\hat{\mathbf{U}}(\boldsymbol{\Lambda}_{\mathrm{H_IB}})^{-1}\hat{\mathbf{V}}^H=\hat{\mathbf{V}}\boldsymbol{\Lambda}_{\mathrm{Z}}\hat{\mathbf{V}}^H$ with $\boldsymbol{\Lambda}_{\mathrm{Z}}=\boldsymbol{\Lambda}_{\mathrm{H_IB}}^2=\mathrm{diag}\left(\frac{1}{\lambda_1},\frac{1}{\lambda_2},\ldots.\frac{1}{\lambda_{\min\{N_{\mathrm{T}},N_{\mathrm{I}}\}}}\right)$.

Moreover, as $\hat{\mathbf{V}}\hat{\mathbf{V}}^H = \hat{\mathbf{I}}$, (42) can be expressed by $\mathbf{F}^* = \hat{\mathbf{V}}\mathbf{\Lambda}_{\mathrm{F}}\hat{\mathbf{V}}^H$, where $\mathbf{\Lambda}_{\mathrm{F}} = \frac{\mu}{\sigma_{\mathrm{I}}^{2N_{\mathrm{I}}}\ln 2}\mathbf{I} - \mathbf{\Lambda}_{\mathrm{Z}}$, i.e.,

$$\mathbf{\Lambda}_{\mathrm{F}} = \mathrm{diag}\Bigg(\left(\frac{\mu}{\sigma_{\mathrm{I}}^{2N_{\mathrm{I}}}\ln 2} - \frac{1}{\lambda_1}\right)^+, \left(\frac{\mu}{\sigma_{\mathrm{I}}^{2N_{\mathrm{I}}}\ln 2} - \frac{1}{\lambda_2}\right)^+, \ldots, \left(\frac{\mu}{\sigma_{\mathrm{I}}^{2N_{\mathrm{I}}}\ln 2} - \frac{1}{\lambda_{\min\{N_{\mathrm{T}},N_{\mathrm{I}}\}}}\right)^+\Bigg). \tag{43}$$

As a result, for given μ and ν, the optimal $\mathbf{Q}^\sharp$ can be given by $\mathbf{Q}^\sharp = \mathbf{B}^{-\frac{1}{2}}\hat{\mathbf{V}}\mathbf{\Lambda}_{\mathrm{F}}\hat{\mathbf{V}}^H\mathbf{B}^{-\frac{1}{2}}$, where μ in (19) should be selected to meet the constraint $\mathrm{Tr}(\mathbf{Q}^*) = P$.

APPENDIX C
THE PROOF OF LEMMA 6

Since $\mathbf{Q}^\sharp$ is a PSD matrix, both $\mathbf{H}\mathbf{Q}^\sharp\mathbf{H}^H$ and $\frac{1}{\sigma^2}(\bar{\mathbf{\Omega}}_\rho^{\frac{1}{2}}\mathbf{H})\mathbf{Q}^\sharp(\bar{\mathbf{\Omega}}_\rho^{\frac{1}{2}}\mathbf{H})^H$ are also PSD matrices. Thus, we may express $\mathbf{H}\mathbf{Q}^\sharp\mathbf{H}^H$ as $\mathbf{H}\mathbf{Q}^\sharp\mathbf{H}^H = \mathbf{D}\mathbf{D}^T$, where $\mathbf{D} \in \mathbb{C}^{N_{\mathrm{T}}\times N_{\mathrm{T}}}$ and express $\frac{1}{\sigma^2}\bar{\mathbf{\Omega}}_\rho^{\frac{1}{2}}\mathbf{H}\mathbf{Q}^\sharp\mathbf{H}^H\bar{\mathbf{\Omega}}_\rho^{\frac{1}{2}}$ as $\frac{1}{\sigma^2}\bar{\mathbf{\Omega}}_\rho^{\frac{1}{2}}\mathbf{H}\mathbf{Q}^\sharp\mathbf{H}^H\bar{\mathbf{\Omega}}_\rho^{\frac{1}{2}} = \frac{1}{\sigma}\bar{\mathbf{\Omega}}_\rho^{\frac{1}{2}}\mathbf{D}\mathbf{D}^T\bar{\mathbf{\Omega}}_\rho^{\frac{1}{2}}\frac{1}{\sigma} = \mathbf{G}\mathbf{G}^T$. Therefore, $\mathbf{G} = \frac{1}{\sigma}\bar{\mathbf{\Omega}}_\rho^{\frac{1}{2}}\mathbf{D} = \frac{1}{\sigma}(\mathbf{I} - \mathbf{\Omega}_\rho)^{\frac{1}{2}}\mathbf{D}$. As a result, $\mathbf{\Omega}_\rho = \mathbf{I} - \sigma^2(\mathbf{G}\mathbf{D}^{-1})^2$. So, $\mathrm{Tr}(\mathbf{\Omega}_\rho\mathbf{H}\mathbf{Q}^\sharp\mathbf{H}^H) = \mathrm{Tr}((\mathbf{I} - (\mathbf{G}\mathbf{D}^{-1})^2)\mathbf{H}\mathbf{Q}^\sharp\mathbf{H}^H) = \mathrm{Tr}((\mathbf{I} - \sigma^2(\mathbf{G}\mathbf{D}^{-1})^2)\mathbf{D}\mathbf{D}^T) = \mathrm{Tr}(\mathbf{D}\mathbf{D}^T - \sigma^2(\mathbf{G}\mathbf{D}^{-1})^2\mathbf{D}\mathbf{D}^T) = \mathrm{Tr}(\mathbf{D}\mathbf{D}^T) - \sigma^2\mathrm{Tr}(\mathbf{G}\mathbf{D}^{-1}\mathbf{G}\mathbf{D}^T)$. Moreover, as $\mathbf{G}\mathbf{D}^{-1} = (\mathbf{I} - \mathbf{\Omega}_\rho)^{\frac{1}{2}}$, which is a diagonal matrix, it can be inferred that $\mathbf{G}\mathbf{D}^{-1} = (\mathbf{G}\mathbf{D}^{-1})^T$. Thus, $\mathrm{Tr}(\mathbf{\Omega}_\rho\mathbf{H}\mathbf{Q}^\sharp\mathbf{H}^H) = \mathrm{Tr}(\mathbf{D}\mathbf{D}^T) - \sigma^2\mathrm{Tr}((\mathbf{D}^{-1})^T\mathbf{G}^T\mathbf{G}\mathbf{D}^T) = \mathrm{Tr}(\mathbf{D}\mathbf{D}^T) - \sigma^2\mathrm{Tr}(\mathbf{G}\mathbf{G}^T) = \mathrm{Tr}(\mathbf{D}\mathbf{D}^T) - \sigma^2\mathrm{Tr}(\mathbf{I} + \mathbf{G}\mathbf{G}^T) + \sigma^2\mathrm{Tr}(\mathbf{I})$, which is a linear function w.r.t. $\mathbf{G}\mathbf{G}^T$. Thus, Problem (33) can be equivalently transformed into

$$\begin{aligned} \max_{\mathbf{G}}\ & \mathrm{Tr}(\mathbf{D}\mathbf{D}^T) - \sigma^2\mathrm{Tr}(\mathbf{I} + \mathbf{G}\mathbf{G}^T) + \sigma^2\mathrm{Tr}(\mathbf{I}) \\ \text{s.t. }\ & \log|\mathbf{I} + \mathbf{G}\mathbf{G}^T| \geq R, \quad \mathbf{G} = \tfrac{1}{\sigma}(\mathbf{I} - \mathbf{\Omega}_\rho)^{\frac{1}{2}}\mathbf{D}, \\ & \mathbf{0} \preceq_{\mathbb{R}_+^{N_{\mathrm{T}}}} \mathbf{\Omega}_\rho \preceq_{\mathbb{R}_+^{N_{\mathrm{T}}}} \mathbf{I}. \end{aligned} \tag{44}$$

Define $\mathbf{W} \triangleq \mathbf{I} + \mathbf{G}\mathbf{G}^T$. Therefore, $\mathbf{W} = \mathbf{I} + (\mathbf{I} - \mathbf{\Omega}_\rho)^{\frac{1}{2}}\mathbf{D}\mathbf{D}^T(\mathbf{I} - \mathbf{\Omega}_\rho)^{\frac{1}{2}}$. As $\mathbf{0} \preceq_{\mathbb{R}_+^{N_{\mathrm{T}}}} \mathbf{\Omega}_\rho \preceq_{\mathbb{R}_+^{N_{\mathrm{T}}}} \mathbf{I}$, it can be inferred that $\mathbf{I} \preceq_{\mathbb{R}_+^{N_{\mathrm{T}}}} \mathbf{W} \preceq_{\mathbb{R}_+^{N_{\mathrm{T}}}} \mathbf{I} + \mathbf{D}\mathbf{D}^T$. So, problem (44) can be further transformed into

$$\begin{aligned} \min_{\mathbf{W}}\ & \sigma^2\mathrm{Tr}(\mathbf{W}) - \mathrm{Tr}(\mathbf{D}\mathbf{D}^T) - \sigma^2\mathrm{Tr}(\mathbf{I}), \\ \text{s.t. }\ & \log|\mathbf{W}| \geq R, \quad \mathbf{I} \preceq_{\mathbb{R}_+^{N_{\mathrm{T}}}} \mathbf{W} \preceq_{\mathbb{R}_+^{N_{\mathrm{T}}}} \mathbf{I} + \mathbf{D}\mathbf{D}^T. \end{aligned} \tag{45}$$

REFERENCES

[1] H. J. Visser and R. J. M. Vullers, "RF energy harvesting and transport for wireless sensor network applications: Principles and requirements," *Proc. IEEE*, vol. 101, no. 6, pp. 1410–1423, Jun. 2013.

[2] M.-L. Ku, W. Li, Y. Chen, and K. J. R. Liu, "Advances in energy harvesting communications: Past, present, and future challenges," *IEEE Commun. Surveys Tuts.*, vol. 18, no. 2, pp. 1384–1412, 2nd Quart., 2016.

[3] S. Ulukus *et al.*, "Energy harvesting wireless communications: A review of recent advances," *IEEE J. Sel. Areas Commun.*, vol. 33, no. 3, pp. 360–381, Mar. 2015.

[4] X. Lu, P. Wang, D. Niyato, D. I. Kim, and Z. Han, "Wireless networks with RF energy harvesting: A contemporary survey," *IEEE Commun. Surveys Tuts.*, vol. 17, no. 2, pp. 757–789, 2nd Quart., 2015.

[5] L. R. Varshney, "Transporting information and energy simultaneously," in *Proc. IEEE ISIT*, Jul. 2008, pp. 1612–1616.

[6] P. Grover and A. Sahai, "Shannon meets Tesla: Wireless information and power transfer," in *Proc. IEEE ISIT*, Jun. 2010, pp. 2363–2367.

[7] R. Zhang and C. K. Ho, "MIMO broadcasting for simultaneous wireless information and power transfer," *IEEE Trans. Wireless Commun.*, vol. 12, no. 5, pp. 1989–2001, May 2013.

[8] I. Krikidis, S. Timotheou, S. Nikolaou, G. Zheng, D. W. K. Ng, and R. Schober, "Simultaneous wireless information and power transfer in modern communication systems," *IEEE Commun. Mag.*, vol. 52, no. 11, pp. 104–110, Nov. 2014.

[9] I.-M. Kim and D. I. Kim, "Wireless information and power transfer: Rate-energy tradeoff for equi-probable arbitrary-shaped discrete inputs," *IEEE Trans. Wireless Commun.*, vol. 15, no. 6, pp. 4393–4407, Jun. 2016.

[10] K. Xiong, C. Chen, G. Qu, P. Y. Fan, and K. B. Letaief, "Group cooperation with optimal resource allocation in wireless powered communication networks," *IEEE Trans. Wireless Commun.*, to be published.

[11] M. Zhang, Y. Liu, and R. Zhang, "Artificial noise aided secrecy information and power transfer in OFDMA systems," *IEEE Trans. Wireless Commun.*, vol. 15, no. 4, pp. 3085–3096, Apr. 2016.

[12] Y. Liu, Z. G. Ding, M. Elkashlan, and H. V. Poor, "Cooperative non-orthogonal multiple access with simultaneous wireless information and power transfer," *IEEE J. Sel. Areas Commun.*, vol. 34, no. 4, pp. 938–953, Apr. 2016.

[13] R. Morsi, D. S. Michalopoulos, and R. Schober, "Multiuser scheduling schemes for simultaneous wireless information and power transfer over fading channels," *IEEE Trans. Wireless Commun.*, vol. 14, no. 4, pp. 1967–1982, Apr. 2015.

[14] X. Zhou, R. Zhang, and C. K. Ho, "Wireless information and power transfer: Architecture design and rate-energy trade-off," *IEEE Trans. Commun.*, vol. 61, no. 11, pp. 4754–4767, Nov. 2013.

[15] H. Lee, S.-R. Lee, K.-J. Lee, H.-B. Kong, and I. Lee, "Optimal beamforming designs for wireless information and power transfer in MISO interference channels," *IEEE Trans. Wireless Commun.*, vol. 14, no. 9, pp. 4810–4821, Sep. 2015.

[16] H. Chen, Y. Li, Y. Jiang, Y. Ma, and B. Vucetic, "Distributed power splitting for SWIPT in relay interference channels using game theory," *IEEE Trans. Wireless Commun.*, vol. 14, no. 1, pp. 410–420, Jan. 2015.

[17] Q. Li, Q. Zhang, and J. Qin, "Secure relay beamforming for simultaneous wireless information and power transfer in nonregenerative relay networks," *IEEE Trans. Veh. Technol.*, vol. 63, no. 5, pp. 2462–2467, Jun. 2014.

[18] K. Xiong, P. Fan, C. Zhang, and K. B. Letaief, "Wireless information and energy transfer for two-hop non-regenerative MIMO-OFDM relay networks," *IEEE J. Sel. Areas Commun.*, vol. 33, no. 8, pp. 1595–1611, Aug. 2015.
I. Krikidis, S. Timotheou, S. Nikolaou, G. Zheng, D. W. K. Ng, and R. Schober, "Simultaneous wireless information and power transfer in modern communication systems," *IEEE Commun. Mag.*, vol. 52, no. 11, pp. 104–110, Nov. 2014.

[19] C.-F. Liu, M. Maso, S. Lakshminarayana, C.-H. Lee, and T. Q. S. Quek, "Simultaneous wireless information and power transfer under different CSI acquisition schemes," *IEEE Trans. Wireless Commun.*, vol. 14, no. 4, pp. 1911–1926, Apr. 2015.

[20] D. W. K. Ng, E. S. Lo, and R. Schober, "Wireless information and power transfer: Energy efficiency optimization in OFDMA systems," *IEEE Trans. Wireless Commun.*, vol. 12, no. 12, pp. 6352–6370, Dec. 2013.

[21] D. W. K. Ng, E. S. Lo, and R. Schober, "Robust beamforming for secure communication in systems with wireless information and power transfer," *IEEE Trans. Wireless Commun.*, vol. 13, no. 8, pp. 4599–4615, Aug. 2014.

[22] Q. Shi, W. Xu, J. Wu, E. Song, and Y. Wang, "Secure beamforming for MIMO broadcasting with wireless information and power transfer," *IEEE Trans. Wireless Commun.*, vol. 14, no. 5, pp. 2841–2853, May 2015.

[23] X. F. Di, K. Xiong, P. Y. Fan, and H.-C. Yang, "Simultaneous wireless information and power transfer in cooperative relay networks with rateless codes," *IEEE Trans. Veh. Technol.*, vol. 66, no. 4, pp. 2981–2996, Apr. 2017.

[24] S. Bi, C. K. Ho, and R. Zhang, "Wireless powered communication: Opportunities and challenges," *IEEE Commun. Mag.*, vol. 53, no. 4, pp. 117–125, Apr. 2015.

[25] J. Xu, L. Liu, and R. Zhang, "Multiuser MISO beamforming for simultaneous wireless information and power transfer," *IEEE Trans. Signal Process.*, vol. 62, no. 18, pp. 4798–4810, Sep. 2014.

[26] Q. Shi, L. Liu, W. Xu, and R. Zhang, "Joint transmit beamforming and receive power splitting for MISO SWIPT systems," *IEEE Trans. Wireless Commun.*, vol. 13, no. 6, pp. 3269–3280, Jun. 2014.
[27] S. Luo, J. Xu, T. J. Lim, and R. Zhang, "Capacity region of MISO broadcast channel for simultaneous wireless information and power transfer," *IEEE Trans. Commun.*, vol. 62, no. 10, pp. 3856–3868, Oct. 2015.
[28] E. Boshkovska, D. W. K. Ng, N. Zlatanov, and R. Schober, "Practical non-linear energy harvesting model and resource allocation for SWIPT systems," *IEEE Commun. Lett.*, vol. 19, no. 12, pp. 2082–2085, Dec. 2015.
[29] E. Boshkovska, R. Morsi, D. W. K. Ng, and R. Schober, "Power allocation and scheduling for SWIPT systems with non-linear energy harvesting model," in *Proc. IEEE ICC*, May 2016, pp. 1–6.
[30] E. Boshkovska, D. W. K. Ng, N. Zlatanov, and R. Schober, "Robust beamforming for SWIPT systems with non-linear energy harvesting model," in *Proc. 17th Int. Workshop Signal Process. Adv. Wireless Commun. (SPAWC)*, Jul. 2016, pp. 1–5.
[31] S. Y. Leng, D. W. K. Ng, N. Zlatanov, and R. Schober, "Multi-objective beamforming for energy-efficient SWIPT systems," in *Proc. IEEE ICNC*, Feb. 2016, pp. 1–7.
[32] Y. J. Dong, M. J. Hossain, and J. L. Chen, "Performance of wireless powered amplify and forward relaying over Nakagami-*m* fading channels with nonlinear energy harvester," *IEEE Commun. Lett.*, vol. 20, no. 4, pp. 672–675, Apr. 2016.
[33] J. L. Zhang and G. F. Pan, "Outage analysis of wireless-powered relaying MIMO systems with non-linear energy harvesters and imperfect CSI," *IEEE Access*, vol. 4, pp. 7046–7053, 2016.
[34] E. Boshkovska, D. W. K. Ng, N. Zlatanov, A. Koelpin, and R. Schober, "Robust resource allocation for MIMO wireless powered communication networks based on a non-linear EH model," *IEEE Trans. Commun.*, vol. 65, no. 5, pp. 1984–1999, May 2017.
[35] T. M. Cover and J. A. Thomas, *Elements of Information Theory*. New York, NY, USA: Wiley, 1991.
[36] S. Boyd and L. Vandenbergh, *Convex Optimization*. Cambridge, U.K.: Cambridge Univ. Press, 2004.
[37] E. Boshkovska, "Practical nonlinear energy harvesting model and resource allocation in SWIPT systems," M.S. thesis, 2016. [Online]. Available: http://arxiv.org/abs/1602.00833
[38] T. Le, K. Mayaram, and T. Fiez, "Efficient far-field radio frequency energy harvesting for passively powered sensor networks," *IEEE J. Solid-State Circuits*, vol. 43, no. 5, pp. 1287–1302, May 2008.
[39] J. Guo and X. Zhu, "An improved analytical model for RF-DC conversion efficiency in microwave rectifiers," in *IEEE MTT-S Int. Microw. Symp. Dig.*, Jun. 2012, pp. 1–3.

Ke Xiong (M'14) received the B.S. and Ph.D. degrees from Beijing Jiaotong University (BJTU), Beijing, China, in 2004 and 2010, respectively. From 2010 to 2013, he was a Post-Doctoral Research Fellow with the Department of Electrical Engineering, Tsinghua University, Beijing. From 2015 to 2016, he was a Visiting Scholar with the University of Maryland, College Park MD, USA. Since 2013, he has been a Lecturer with BJTU, where he is currently an Associate Professor with the School of Computer and Information Technology. He has published over 60 academic papers in referred journals and conferences. His current research interests include wireless cooperative networks, wireless powered networks, and network information theory. He is a member of China Computer Federation and also a senior member of the Chinese Institute of Electronics. He serves as an Associate Editor-in Chief of the Chinese journal *New Industrialization Strategy*, and an Editor of *Computer Engineering and Software*. In 2017, he serves as the Leading Editor of the Special issue Recent Advances in Wireless Powered Communication Networks for *EURASIP Journal on Wireless Communications and Networking*. He also serves as a Reviewer for over 15 international journals, including IEEE TRANSACTIONS ON SIGNAL PROCESSING, IEEE TRANSACTIONS ON WIRELESS COMMUNICATIONS, IEEE TRANSACTIONS ON COMMUNICATIONS, IEEE TRANSACTIONS ON VEHICULAR TECHNOLOGY, IEEE COMMUNICATION LETTERS, IEEE SIGNAL PROCESSING LETTERS, and IEEE WIRELESS COMMUNICATION LETTERS. He also served as the Session Chair of the IEEE GLOBECOM2012, the IET ICWMMN2013, the IEEE ICC2013, the ACM MOMM2014, and the Publicity and Publication Chair of the IEEE HMWC2014, as well as the TPC Co-Chair of the IET ICWMMN2017.

Beibei Wang (SM'15) received the B.S. degree (Hons.) in electrical engineering from the University of Science and Technology of China, Hefei, in 2004, and the Ph.D. degree in electrical engineering from the University of Maryland at College Park , College Park, MD, USA, in 2009. She was with the University of Maryland as a Research Associate from 2009 to 2010, and with Qualcomm Research and Development from 2010 to 2014. Since 2015, she has been with Origin Wireless Inc. as a Principal Technologist. She has coauthored the book *Cognitive Radio Networking and Security: A Game-Theoretic View* (Cambridge University Press, 2010). Her research interests include wireless communications and signal processing. She received the Graduate School Fellowship, the Future Faculty Fellowship, and the Deans Doctoral Research Award from the University of Maryland, and the Overview Paper Award from the IEEE Signal Processing Society in 2015.

K. J. Ray Liu (F'03) was a Distinguished Scholar-Teacher with the University of Maryland, College Park, MD, USA, in 2007, where he is currently the Christine Kim Eminent Professor of Information Technology and leads the Maryland Signals and Information Group conducting research encompassing broad areas of information and communications technology with recent focus on smart radios for smart life.

Dr. Liu is a fellow of AAAS. He was a recipient of the 2016 IEEE Leon K. Kirchmayer Technical Field Award on graduate teaching and mentoring, the IEEE Signal Processing Society 2014 Society Award, and the IEEE Signal Processing Society 2009 Technical Achievement Award. He is recognized by Thomson Reuters as a Highly Cited Researcher. He is a member of the IEEE Board of Directors. He was a President of the IEEE Signal Processing Society, where he has served as a Vice President C Publications and Board of Governor. He has also served as the Editor-in-Chief of *IEEE Signal Processing Magazine*.

He also received teaching and research recognitions from the University of Maryland, including the university-level Invention of the Year Award, the college-level Poole and Kent Senior Faculty Teaching Award, the Outstanding Faculty Research Award, and the Outstanding Faculty Service Award, all from the A. James Clark School of Engineering.